School of Mathematical
and Physical Sciences

University of Reading

Department of Mathematics and Statistics

Preprint MPS-2012-10

28 March 2012

High frequency sound propagation in a network of interconnecting streets

by

D. P. Hewett

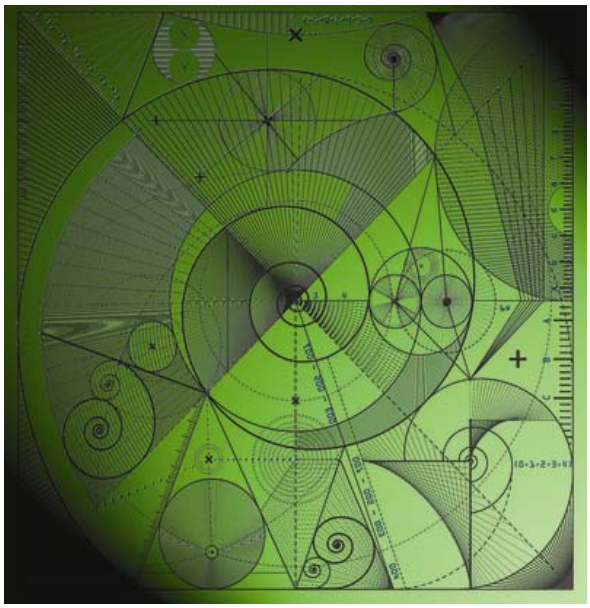

High frequency sound propagation in a network of interconnecting streets

D. P. Hewett*,a,1

[a] *Oxford Centre for Industrial and Applied Mathematics (OCIAM), Mathematical Institute, 24–29 St. Giles, Oxford OX1 3LB, UK*

Abstract

We propose a new model for the propagation of acoustic energy from a time-harmonic point source through a network of interconnecting streets in the high frequency regime, in which the wavelength is small compared to typical macro-lengthscales such as street widths/lengths and building heights. Our model, which is based on geometrical acoustics (ray theory), represents the acoustic power flow from the source along any pathway through the network as the integral of a power density over the launch angle of a ray emanating from the source, and takes into account the key phenomena involved in the propagation, namely energy loss by wall absorption, energy redistribution at junctions, and, in 3D, energy loss to the atmosphere. The model predicts strongly anisotropic decay away from the source, with the power flow decaying exponentially in the number of junctions from the source, except along the axial directions of the network, where the decay is algebraic.

Key words: Urban Acoustics, Frequency Domain, High Frequency, Multiple Scattering.

1. Introduction

The main difficulties arising in a mathematical study of urban sound propagation are due to the complex geometry of the propagation domain. The presence of multiple scatterers such as buildings, vegetation, vehicles, pedestrians and street furniture, all of which have different acoustical scattering properties, serves to create an extremely complicated sound field, an exact description of which, either analytical or numerical, is usually impossible.

Broadly speaking, the effect of domain complexity occurs on two distinct lengthscales. On the 'microscale' we have the effects of wall absorption, scattering by wall inhomogeneities, and scattering by the obstacles present in each street. On the 'macroscale' we may view an urban environment as a network of streets and junctions, through which acoustic energy propagates.

The existing urban acoustics literature focuses mainly on the modelling of microscale effects, in particular on the accurate prediction of the sound field in a single street. Even in the absence of traffic, pedestrians, vegetation and street furniture this presents a major challenge, because of the

*Tel. +44 118 3785012

Email address: d.p.hewett@reading.ac.uk (D. P. Hewett)

[1]Present address: Department of Mathematics, University of Reading, Whiteknights, PO Box 220, Reading RG6 6AX, UK

absorbent and inhomogeneous nature of building facades. A number of different models have been proposed, some based on ray theory [1, 2, 3, 4, 5], others on modal decomposition [6, 7] and others on transport and diffusion approximations [8, 9] - for a more detailed overview see e.g. [10, 11, 12, 13].

The difficulty of the microscale problem has meant that relatively little theoretical work has been published on the macroscale problem of propagation in environments involving multiple streets, and this is the problem we address in this paper. Specifically, we consider the propagation of acoustic energy from a time-harmonic point source in a network of interconnecting streets, in the high frequency regime where the wavelength is small compared to typical macro-lengthscales such as street lengths and widths. In order to facilitate study of the macroscale problem we adopt a rather simple microscale model, in which building facades are assumed to be homogeneous, the scattering effect of obstacles inside streets is neglected, and metereological effects are ignored.

Our objective is to calculate the acoustic power flow down each street in the network. Our method is based on geometrical acoustics (ray theory), with both the interference between ray fields and diffraction effects being neglected. We shall show how the acoustic power flow across a street cross-section can be approximated by an integral over a ray-angle-resolved power density. A key component in our analysis is a careful study of the redistribution of acoustic energy incident at a typical junction between streets. This single-junction problem has been studied previously in [14, 15], the latter work being in the context of modelling sound propagation along office corridors. However, to the best of our knowledge the results of [14, 15] have not been extended to domains involving more than one junction, until now.

The structure of the paper is as follows. §2 reviews the ray-theoretical model of acoustic energy propagation that will be used. §3 applies this model to the case of a single 2D street, and shows that, under certain assumptions, the acoustic power flow across a street cross-section far from the source can be approximated by an integral over a ray-angle-resolved power density. §4 derives similar integral approximations to the power flows out of the exits of a junction between two 2D streets. §5 extends the method to the calculation of power flows along pathways involving multiple junctions. §6 concerns the calculation of the power flows through a network of interconnecting 2D streets, and shows how the problem can be reformulated as a coupled system of partial difference equations, with an exact solution of this system being derived in a special case. §7 demonstrates the applicability of our 2D model to the prediction of sound propagation in a network of 3D corridors, comparing our results to those in [15]. Finally, §8 describes the generalisation of the 2D model to a 3D urban environment.

2. Ray theory and energy propagation

We assume that the propagation is described by a velocity potential $\Phi(\mathbf{x}, t)$ satisfying

$$\frac{\partial^2 \Phi}{\partial t^2}(\mathbf{x}, t) = c_0^2 \nabla^2 \Phi(\mathbf{x}, t),$$

where c_0 is the propagation speed, and $\Phi(\mathbf{x}, t)$ is related to the velocity and pressure perturbations $\mathbf{u}(\mathbf{x}, t)$ and $p(\mathbf{x}, t)$ in the acoustic approximation by

$$\mathbf{u}(\mathbf{x}, t) = \boldsymbol{\nabla} \Phi(\mathbf{x}, t), \qquad \rho_0 \frac{\partial \Phi}{\partial t}(\mathbf{x}, t) + p(\mathbf{x}, t) = 0, \tag{1}$$

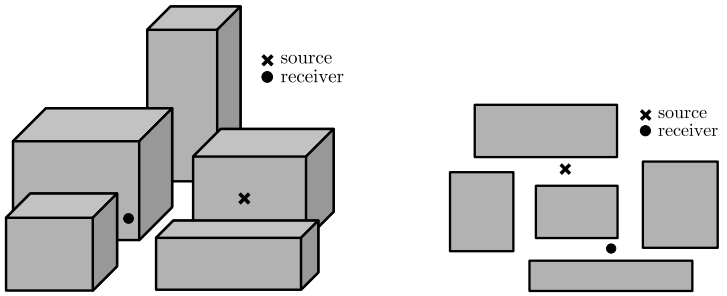

(a) 3D model (b) 2D model

Figure 1: 3D and 2D models of an urban environment.

where ρ_0 is the equilibrium density. For time-harmonic waves we assume that $\Phi(\mathbf{x}, t) = \mathrm{Re}[\phi(\mathbf{x})\mathrm{e}^{-\mathrm{i}\omega t}]$ for some angular frequency $\omega > 0$. Then, assuming a point source, $\phi(\mathbf{x})$ satisfies the Helmholtz equation

$$(\nabla^2 + k^2)\phi(\mathbf{x}) = A\,\delta(\mathbf{x} - \mathbf{x}_0), \tag{2}$$

where $\mathbf{x}_0$ is the source location, A is its amplitude, and $k = \omega/c_0$ is the wavenumber.

In order to simplify the microscale features as much as possible, we model buildings as homogeneous polyhedral blocks on a flat plane ground (see Figure 1(a)). We also consider the analogous 2D problem, where buildings are modelled as polygons rather than polyhedra (see Figure 1(b)). To begin with, the rigid (sound-hard) boundary condition

$$\frac{\partial \Phi}{\partial \mathbf{n}}(\mathbf{x}) = 0 \tag{3}$$

is assumed on the walls, roofs and ground (where applicable), where $\mathbf{n}$ is the outward unit normal vector. The boundary condition (3) is a reasonable first approximation given that most building materials are very good reflectors of sound energy [16]. In reality, a small amount of energy will be absorbed at each reflection, and later in this section we introduce a simple absorption coefficient model to take this into account.

The exact analytical solution of (2)-(3) is impossible except in a small number of very simple geometries. At relatively low frequencies, numerical methods (e.g. the finite element method) can be applied to obtain approximate solutions. However, in the high frequency regime in which $kL = \omega L/c_0 \gg 1$, where L is a typical distance between buildings, the highly oscillatory nature of the wave solution ϕ means that a full numerical solution is usually infeasible. In this case one can apply asymptotic methods, such as geometrical acoustics, and the geometrical theory of diffraction (see e.g. [17, 18]), to obtain approximate solutions in which the wave field is represented as a sum of ray fields. These methods reduce the calculation of the wave solution to the (not always trivial) problem of determining all of the rays (incident, reflected, diffracted) between source and receiver, and summing their respective contributions.

But for practical purposes, it is important to note that in the high frequency regime the precise details of the wave solution are highly sensitive to changes in geometry, such as street widths or lengths and source or receiver locations. In applications, such characteristics are usually known only to a certain degree of accuracy, and may best be considered random variables. Hence, even if

a numerical or asymptotic calculation of the full wave solution in one particular realisation of the domain could be achieved, it would be of limited practical relevance [19, 20].

A more robust measure of the broad spatial variation of the sound field can be obtained by studying the distribution of *acoustic energy* across the domain (cf. e.g. [1, 3, 6]) . The acoustic energy and the associated *acoustic intensity* are 'quadratic' quantities (i.e. they involve products of two 'small' perturbations in the acoustic approximation), which can be averaged both temporally and spatially to provide measures of the magnitude of the sound field that are less sensitive to perturbations in the domain characteristics than are the full details of the wave solution. The *instantaneous acoustic energy density* W and *acoustic intensity* $\mathbf{I}$ are defined by [21]

$$W(\mathbf{x},t) := \frac{1}{2}\rho_0|\mathbf{u}(\mathbf{x},t)|^2 + \frac{1}{2}\frac{(p(\mathbf{x},t))^2}{\rho_0 c_0^2}, \qquad \mathbf{I}(\mathbf{x},t) := p(\mathbf{x},t)\mathbf{u}(\mathbf{x},t), \tag{4}$$

and satisfy the equation of conservation of acoustic energy

$$\frac{\partial W}{\partial t} = -\nabla\cdot\mathbf{I},$$

so that $\mathbf{I}$ describes the instantaneous acoustic energy flux at a given point in space. In the time-harmonic case we remove the temporal oscillations by averaging (4) over one period of oscillation. Denoting the resulting quantities by $\langle W\rangle(\mathbf{x})$ and $\langle\mathbf{I}\rangle(\mathbf{x})$, we find, using (1), that

$$\langle W\rangle(\mathbf{x}) = \frac{\rho_0}{4}\left(\boldsymbol{\nabla}\phi(\mathbf{x})\cdot\overline{\boldsymbol{\nabla}\phi(\mathbf{x})} + k^2\phi(\mathbf{x})\overline{\phi(\mathbf{x})}\right), \qquad \langle\mathbf{I}\rangle(\mathbf{x}) = \frac{\rho_0\omega}{2}\,\mathrm{Im}[\overline{\phi}(\mathbf{x})\boldsymbol{\nabla}\phi(\mathbf{x})], \tag{5}$$

where the overbar denotes complex conjugation. The time-averaged acoustic energy flux (or *power flow*) P across a surface S is given by the integral

$$P = \int_S \langle\mathbf{I}\rangle\cdot\mathbf{n}\,dS, \tag{6}$$

where $\mathbf{n}$ is the positively-oriented unit normal vector to S.

In the high frequency regime, (5) can be simplified further. Indeed, when ϕ is described by a single ray field, $\langle W\rangle$ and $|\langle\mathbf{I}\rangle|$ are simply proportional to $|\phi|^2$, with $\langle\mathbf{I}\rangle$ pointing in the ray direction [10, §3.4.2]. Furthermore, the acoustic energy is proportional to $\langle p^2\rangle$, the *mean-square pressure*, with

$$\langle p^2\rangle \sim \rho_0 c_0^2\langle W\rangle. \tag{7}$$

More generally, when ϕ is approximated by a sum of ray fields, we will make the standard simplifying assumption (see e.g. [1, 22, 23]) that acoustic energy and intensity can be computed by 'incoherently' summing the energies/intensities associated with each of the individual ray fields. That is, we neglect interference between ray fields. We remark that, under this assumption, the same relationship (7) between the acoustic energy and the mean-square pressure holds as for a single ray field.

We refer to the resulting model as the *ray model of acoustic energy propagation*, or simply the *ray model* for short. In a highly reverberant environment for which there is some uncertainty in domain characteristics, the validity of the ray model can be justified by assuming that the phases of each of the ray fields are independent random variables, so that the expected contribution of interference terms is zero in the ensemble average. This reasoning has similarities to the method

of 'Statistical Energy Analysis' (SEA), a technique used to predict the distribution of vibrational energy in complex mechanical structures (see e.g. [20, 24]). Even in the fully deterministic case, it is sometimes possible to justify the neglect of interference effects by performing some sort of spatial averaging over either the source or receiver location, provided that the averaging region is chosen so that the interference terms oscillate sufficiently to average to zero in the high frequency limit. In [10, §3.5] this statement is verified in the case of a single 2D street, with the averaging region chosen to be a street cross-section. To be precise, in [10] the acoustic power flow down the street is studied, and it is shown that the prediction of the ray model does indeed approximate the exact power flow in the high frequency limit, provided that the source is not too close to either of the street walls and that resonance effects are dealt with appropriately.

The boundary condition (3) assumes that the street walls are perfectly reflecting, and leads to the familiar specular ray reflection law "angle of incidence equals angle of reflection". In practice, some energy incident on the walls is absorbed, and the simplest way of including this in the ray model (cf. [1, 4]) is to introduce an *absorption coefficient* $\alpha \in [0, 1]$, such that the magnitude I of the intensity along a ray undergoing a reflection at the boundary is attenuated according to the rule

$$I_{\text{reflected}} = (1 - \alpha)\, I_{\text{incident}}.$$

As a first approximation, we take α to be independent of the angle of incidence/reflection. The relationship between this simple ray-based absorption model and full wave-based models such as impedance boundary conditions is rather subtle (see e.g. [25, 26, 27, 28]), and will not be discussed here. However, we remark that the form of the integral approximations derived in this paper would make generalisation to angle-dependent absorption coefficients a possibility for future work.

Experimental studies have shown that the absorption coefficient of a material depends weakly on the wavelength of the incident wave [16, Chapter 57]. Most common building materials are very good reflectors of sound, with the value of α at normal incidence and in the high frequency range typically lying in the range $0 < \alpha < 0.1$. For example, $\alpha = 0.04$ for an unpainted brick wall and $\alpha = 0.02$ for a painted brick wall at 1KHz [16, p. 708]. In practice, the absorption coefficient may vary along the street depending on the nature of the building facades, but for simplicity we assume that the effects of wall absorption can be represented by an effective absorption coefficient that is a known characteristic of each street.

3. A single 2D street

We consider first the case of a single 2D street bounded by infinite parallel rigid walls. After nondimensionalising lengths relative to the street width, we may assume that the walls are at $y = 0$ and $y = 1$, with the source located at the point $(0, y_0)$, $0 < y_0 < 1$. Then ϕ satisfies

$$(\nabla^2 + k^2)\phi(x, y) = A\delta(x)\delta(y - y_0), \qquad -\infty < x < \infty,\ 0 < y < 1, \tag{8}$$

$$\frac{\partial \phi}{\partial y}(x, y) = 0, \qquad y = 0, 1, \tag{9}$$

where k is the nondimensional wavenumber, along with the requirement that ϕ should represent waves which propagate outward at $x = \pm\infty$. An exact representation of the solution can be

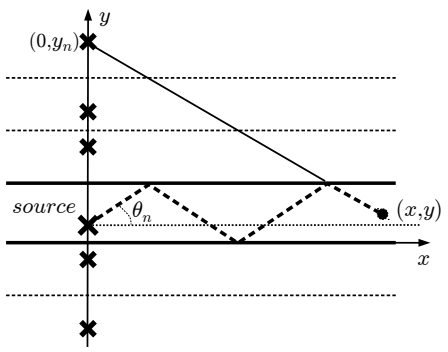

Figure 2: Association between image sources and rays in a single 2D street.

constructed by the method of images. Introducing an infinite array of image sources at the points $(0, y_n)$, $n \in \mathbb{Z} \setminus \{0\}$, where

$$y_n = \begin{cases} n + y_0, & n \text{ even}, \ n \neq 0, \\ n + (1 - y_0), & n \text{ odd}, \end{cases} \tag{10}$$

a formal solution of (8) satisfying the boundary conditions (9) can be obtained by setting

$$\phi(x, y) = \sum_{n \in \mathbb{Z}} \phi_n(x, y), \tag{11}$$

where $\phi_n(x, y)$ is the free space velocity potential associated with each of the image sources,

$$\phi_n(x, y) = -A \frac{\mathrm{i}}{4} H_0^{(1)}(k\sqrt{x^2 + (y - y_n)^2}).$$

The sum (11) is convergent whenever $k \notin \pi\mathbb{N}$, i.e. away from resonance.

The geometrical acoustics approximation is an infinite sum of ray fields, each being the far-field approximation of the Hankel function associated with one of the image sources. As Figure 2 illustrates, the contribution of each image source $(0, y_n)$ can be associated with exactly one ray emanating from the physical source, with launch angle θ_n given by

$$\theta_n(x, y) = \begin{cases} \operatorname{sgn}(n)(-1)^n \arctan\left(\frac{y_n - y}{x}\right), & n \neq 0, \\ -\arctan\left(\frac{y_0 - y}{x}\right), & n = 0. \end{cases}$$

According to the ray model, the acoustic power flow P across a street cross-section at distance x from the source is equal to the incoherent sum of the free space power flows across the street cross-section from each of the image sources. As a fraction of the total free space power output of the source (we shall adopt this normalisation for the remainder of the paper), the power flow from the nth image source is equal to $1/(2\pi)$ times the angular width $\Theta_n = \Theta_n(x, y_0)$ of the tube of rays from the image source that intersect the street cross-section at x (see Figure 3(a)), and

$$P(x) = \frac{1}{2\pi} \sum_{n \in \mathbb{Z}} (1 - \alpha)^{|n|} \Theta_n. \tag{12}$$

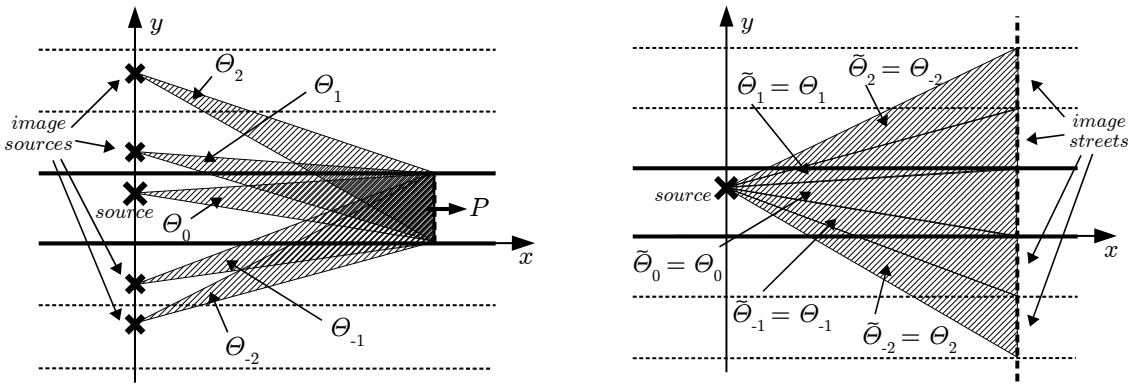

(a) Image sources

(b) Image streets

Figure 3: The geometrical interpretation of Θ_n and $\tilde{\Theta}_n$ in a single 2D street.

It is convenient to rewrite (12) as

$$P(x) = \frac{1}{2\pi} \sum_{n \in \mathbb{Z}} (1-\alpha)^{|n|} \tilde{\Theta}_n, \tag{13}$$

where

$$\tilde{\Theta}_n = \begin{cases} \Theta_{-n}, & n \text{ even}, \\ \Theta_n, & n \text{ odd}. \end{cases} \tag{14}$$

Explicitly, $\tilde{\Theta}_n = \tilde{\theta}_n^+ - \tilde{\theta}_n^-$, where

$$\tilde{\theta}_n^+ = \arctan \frac{n+1-y_0}{x}, \qquad \tilde{\theta}_n^- = \arctan \frac{n-y_0}{x}. \tag{15}$$

Geometrically, the transformation of (12) into (13) corresponds to moving all the image sources (and their respective ray tubes) to the point $(0, y_0)$ and considering the total power flow from a single source located at that point across an infinite array of *image street* cross-sections (i.e. across the line $\{x\} \times (-\infty, \infty)$). After reflecting the ray tubes corresponding to the odd-indexed image sources in the line $y = y_0$ we obtain the picture in Figure 3(b). This image street construction will prove useful in subsequent calculations.

Noting that $\tilde{\theta}_n^+ = \tilde{\theta}_{n+1}^-$, we see that, in the special case $\alpha = 0$ (perfectly reflecting walls), (13) is a telescoping sum which collapses to give

$$P = \frac{1}{2\pi} \left(\arctan(\infty) - \arctan(-\infty) \right) = \frac{1}{2}. \tag{16}$$

Note that (16) is independent of the distance x down the street, and that (as we would expect) the combined contribution from all the image sources is simply the total free space power output in the positive x-direction of a source at the point $(0, y_0)$.

3.1. Asymptotic behaviour far from the source

When $\alpha \neq 0$, the power flow down the street is no longer independent of x. The asymptotic behaviour of (13) when the receiver is far from the source ($x \gg 1$) depends on the size of the

absorption coefficient. When $\alpha \gg 1/x$, the main contribution to the sum comes from near $n = 0$, and [10, §3.5.2]

$$P(x) \sim \frac{2-\alpha}{2\pi\alpha x}\left(1 + \frac{1}{x^2}\left(y_0(1-y_0) - \frac{1}{3} - \frac{2(1-\alpha)}{\alpha^2}\right) + O\left(\frac{1}{x^4}\right)\right), \quad x \to \infty,\ \alpha \gg 1/x. \tag{17}$$

To deal with the case $\alpha = O(1/x)$, we first use the identity

$$\arctan z_1 \pm \arctan z_2 = \arctan \frac{z_1 \pm z_2}{1 \mp z_1 z_2} \tag{18}$$

to deduce that

$$\tilde{\Theta}_n = \arctan \frac{1}{x + \frac{(n+1-y_0)(n-y_0)}{x}} \sim \frac{1}{x + \frac{n^2}{x}}\left(1 + O\left(\frac{1}{x}\right)\right), \quad x \to \infty, \tag{19}$$

uniformly for all n. Inserting (19) into (13) then gives

$$P(x) \sim \frac{1}{2\pi}\left(-\frac{1}{x} + \frac{2}{x}\sum_{n=0}^{\infty}(1-\alpha)^n \frac{1}{1+\frac{n^2}{x^2}}\right), \quad x \to \infty, \tag{20}$$

and, replacing the sum in (20) by an integral, we find that

$$P(x) \sim \frac{1}{\pi}\int_0^{\infty} \frac{(1-\alpha)^{xt}}{1+t^2}\,dt + O\left(\frac{1}{x}\right), \quad x \to \infty,\ \alpha = O(1/x). \tag{21}$$

In fact, (21) is valid not just for $\alpha = O(1/x)$, but for all $\alpha \ll 1$. Indeed, when $1/x \ll \alpha \ll 1$ (21) is a Laplace-type integral with leading order behaviour

$$\frac{1}{\pi}\int_0^{\infty} \frac{(1-\alpha)^{xt}}{1+t^2}\,dt \sim \frac{1}{\pi\alpha x},$$

which clearly agrees with the leading order term in (17) when $1/x \ll \alpha \ll 1$. Since in applications the absorption coefficient can usually be considered a small parameter (cf. §2), we focus exclusively on the regime $\alpha \ll 1$ from now on.

3.2. Interpretation in terms of ray angles

The integral approximation (21) can be written in a number of ways - for example, in terms of exponential integrals. A particularly useful representation is obtained via the change of variable $t = \tan\theta$, which gives

$$P(x) \sim \frac{1}{\pi}\int_0^{\pi/2} (1-\alpha)^{x\tan\theta}\,d\theta, \quad x \to \infty,\ \alpha \ll 1. \tag{22}$$

The integration variable θ may be identified with the absolute value of the launch angle of a ray emanating from the source (cf. Figure 2), and (22) then states that the power flow far from the source can be computed as an integral over launch angles of a 'power density' propagating at each value of θ, after attenuation by wall absorption. The exponent $x\tan\theta$ in the integrand represents a continuous approximation to the discrete number of reflections undergone by a ray of launch angle $\pm\theta$. This interpretation will offer considerable insight when we come to study the way that the energy propagating along a street is redistributed at a junction with another street.

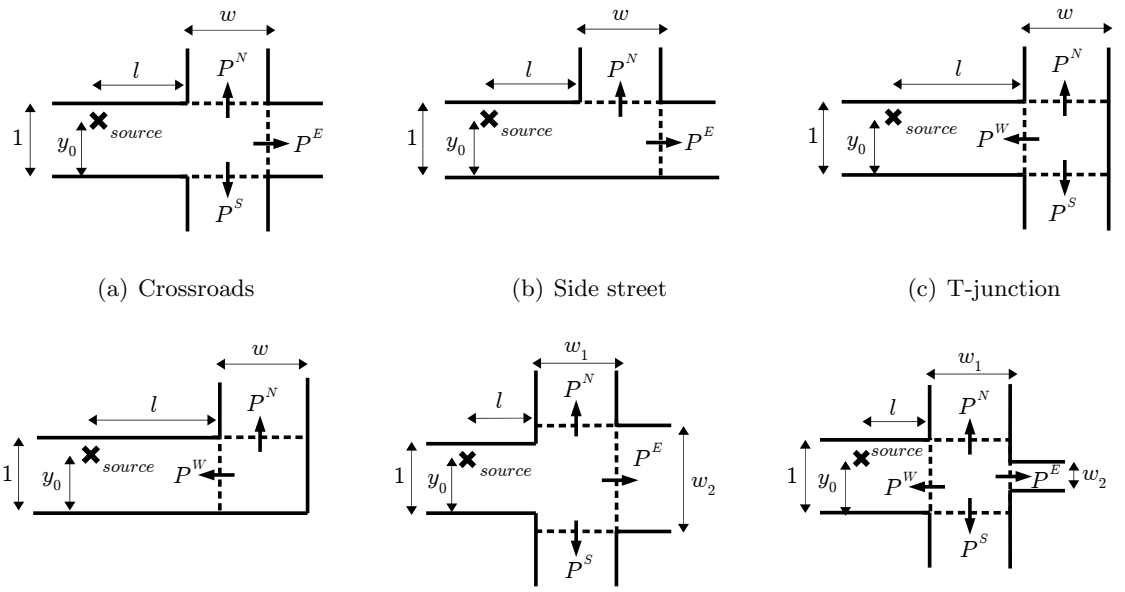

(a) Crossroads (b) Side street (c) T-junction

(d) Right-angled bend (e) Asymmetric crossroads ($w_2 > 1$) (f) Asymmetric crossroads ($w_2 < 1$)

Figure 4: Common junction types

4. Energy redistribution at a junction in 2D

4.1. Energy redistribution at a crossroads

We begin with the case of a right-angled crossroads, as illustrated in Figure 4(a). As in §3, we nondimensionalise lengths so that the width of the street containing the source is equal to 1. In the high frequency regime, the geometrical theory of diffraction represents the sound field as the sum over all of the geometrical rays that exist between source and receiver. These rays can be put into two categories: those rays which involve either direct propagation or one or more reflections at the street walls, and those which involve diffraction at one or more of the sharp edges of the junction. The field due to the latter constitutes a higher-order correction to the field due to the former, and, as a first approximation, we propose to estimate the acoustic power flows P^N, P^E and P^S out of the North, East and South exits of the junction by neglecting diffraction effects and considering the contribution of the incident and (multiply-)reflected ray fields alone.

The validity of this model is discussed in detail in [10, §3.6.1.1]; roughly speaking, we expect the model to be valid only over propagation distances that are shorter than the *Rayleigh distance* (sometimes called the *Fresnel distance*) kw^2, where k is the dimensional wavenumber and w is a typical street width. For example, in downtown Manhattan, New York City, measurements from satellite photographs suggest that w lies in the range $w \in (20\text{m}, 40\text{m})$, and, at a typical frequency of 1kHz, which corresponds to a spatial wavelength of around 30cm, and a dimensional wavenumber $k \approx 20\text{m}^{-1}$, the Rayleigh distance is approximately 18000m. This is considerably larger than the typical street length l, which appears to lie in the range $l \in (100\text{m}, 200\text{m})$, and the neglect of diffraction effects is therefore justified, at least within a few blocks of the source. However, for narrower streets, longer propagation distances or at lower frequencies, a more careful treatment of the diffraction effects may be required (see e.g. [29, 30]).

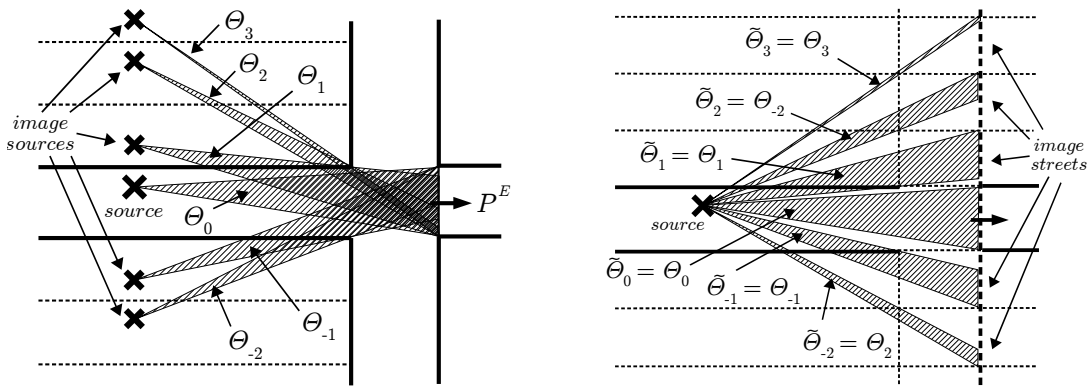

(a) Image sources (b) Image streets

Figure 5: The geometrical interpretation of Θ_n and $\tilde{\Theta}_n$ at a crossroads.

The power flow P^E out of the East exit of the junction is then computed by incoherently summing the power flows along the ray tubes reaching the exit from each of the image sources defined in (10), so that

$$P^E = \frac{1}{2\pi} \sum_{n \in \mathbb{Z}} (1-\alpha)^{|n|} \Theta_n, \tag{23}$$

where α is the absorption coefficient of the street containing the source and $\Theta_n = \Theta_n(l, w, y_0)$ is the angular width of the tube of rays from the nth image source that reach the East exit (see Figure 5(a)). Since only a finite number of image sources have a 'line-of-sight' to the East exit, (23) is actually a finite sum, which can be rewritten in terms of the image street representation (see Figure 5(b)) as

$$P^E = \frac{1}{2\pi} \sum_{n=-\left\lfloor \frac{l}{w}+1-y_0 \right\rfloor}^{\left\lfloor \frac{l}{w}+y_0 \right\rfloor} (1-\alpha)^{|n|} \tilde{\Theta}_n, \tag{24}$$

where $\tilde{\Theta}_n = \tilde{\theta}_n^+ - \tilde{\theta}_n^-$ and

$$\tilde{\theta}_n^+ = \begin{cases} \arctan \frac{n+1-y_0}{l+w}, & 0 \le n \le \left\lfloor \frac{l}{w} + y_0 \right\rfloor, \\ \arctan \frac{n+1-y_0}{l}, & -\left\lfloor \frac{l}{w} + 1 - y_0 \right\rfloor \le n < 0, \end{cases} \qquad \tilde{\theta}_n^- = \begin{cases} \arctan \frac{n-y_0}{l}, & 0 < n \le \left\lfloor \frac{l}{w} + y_0 \right\rfloor, \\ \arctan \frac{n-y_0}{l+w}, & -\left\lfloor \frac{l}{w} + 1 - y_0 \right\rfloor \le n \le 0. \end{cases} \tag{25}$$

We now consider the behaviour of (24) in the limit $l \to \infty$. By (18),

$$\tilde{\Theta}_n = \begin{cases} \arctan \frac{l+w(n+1-y_0)}{l(l+w)+(n+1-y_0)(n-y_0)}, & -\left\lfloor \frac{l}{w} + 1 - y_0 \right\rfloor \le n \le -1, \\ \arctan \frac{l+w}{(l+w)^2 - y_0(1-y_0)}, & n = 0, \\ \arctan \frac{l-w(n-y_0)}{l(l+w)+(n+1-y_0)(n-y_0)}, & 1 \le n \le \left\lfloor \frac{l}{w} + y_0 \right\rfloor, \end{cases}$$

so that, uniformly for all n,

$$\tilde{\Theta}_n \sim \frac{1 - |\frac{wn}{l}|}{l + \frac{n^2}{l}} \left(1 + O\left(\frac{1}{l} \right) \right), \quad l \to \infty, \ w = O(1). \tag{26}$$

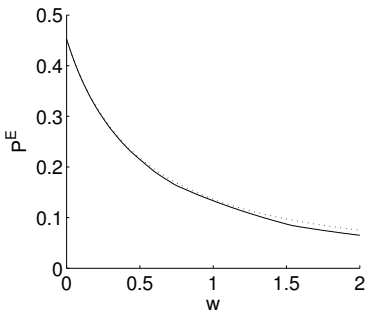

Figure 6: Comparison of ray tube sum (24) (solid line) and the corresponding integral approximation (27) (dotted line) for the power flow past a crossroads, plotted against the side street width w. Here $l = 2$, $y_0 = 0.3$, $\alpha = 0.02$.

Inserting (26) into (24) and approximating the sum by an integral, we find that

$$P^E \sim \frac{1}{\pi}\int_0^{1/w} (1-\alpha)^{lt}\frac{1-wt}{1+t^2}\,dt + O\left(\frac{1}{l}\right), \quad l\to\infty,\ w = O(1),\ \alpha = O(1/l). \tag{27}$$

In fact, as before, (27) can be shown to be valid for all $\alpha \ll 1$ (see [10, §3.6.1.2]).

Approximations to the power flows P^N and P^S can be obtained similarly. The ray tube summations are now infinite, with P^N being a sum solely over the image sources $n \le 0$ and P^S being a sum solely over the image sources $n \ge 0$. For $\alpha \ll 1$, both P^N and P^S are found to have the same leading order asymptotic behaviour

$$P^N \sim P^S \sim \frac{1}{2\pi}\left(\int_0^{1/w} (1-\alpha)^{lt} wt\,dt + \int_{1/w}^{\infty} (1-\alpha)^{lt}\,dt\right), \quad l\to\infty,\ w = O(1),\ \alpha \ll 1. \tag{28}$$

We remark that although our integral approximations were derived for $l \to \infty$, good agreement with numerical evaluations of the ray tube sums is observed even when l is not particularly large. For example, Figure 6 shows a comparison between (24) and (27) for $l = 2$.

4.2. Interpretation in terms of ray angles

The approximations (27) and (28) can be rewritten by the change of variable $t = \tan\theta$ as

$$P^E \sim \frac{1}{\pi}\int_0^{\pi/2} (1-\alpha)^{l\tan\theta} F_C(\theta; w)\,d\theta, \qquad l\to\infty,\ w = O(1),\ \alpha \ll 1, \tag{29}$$

$$P^N \sim P^S \sim \frac{1}{\pi}\int_0^{\pi/2} (1-\alpha)^{l\tan\theta} F_T(\theta; w)\,d\theta, \qquad l\to\infty,\ w = O(1),\ \alpha \ll 1, \tag{30}$$

where

$$F_C(\theta; w) := \max\{1 - w\tan\theta, 0\}, \qquad F_T(\theta; w) := \frac{1}{2}\min\{w\tan\theta, 1\}.$$

As in §3.2, we identify θ with the absolute value of the launch angle of a ray emanating from the source, and interpret the integrands in (29) and (30) as θ-resolved power densities. The functions $F_C(\theta; w)$ and $F_T(\theta; w)$ (which are plotted in Figure 7 for a fixed value of the side street width w)

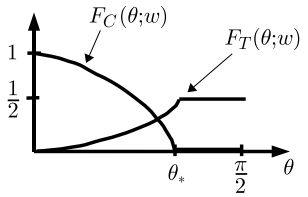

Figure 7: The functions F_C and F_T

describe the way that the power density incident on the junction at a given value of θ is redistributed between the exits of the junction: $F_C(\theta; w)$ gives the proportion of the power density that crosses the junction, flowing out of the East exit, and $F_T(\theta; w)$ gives the proportion that 'turns the corner' and flows out of each of the North and South exits. The fact that $F_C(\theta; w) = 0$ for $\theta > \theta_* := \arctan 1/w$ reflects the geometrical fact that any ray with launch angle greater than θ_* must leave the junction by either the North or South exit.

4.3. Probabilistic interpretation

The functions $F_C(\theta; w)$ and $F_T(\theta; w)$ can also be interpreted as probability densities. A ray emanating from the source with launch angle θ has, upon reaching the junction, a certain offset $q \in (0, 1)$ from the bottom wall of the main street and a certain orientation $O = \pm 1$, depending on the sign of the angle between the ray and the horizontal. In the limit $l \to \infty$, the rays in a narrow ray tube of fixed width $d\theta$ around the launch angle θ have their offsets and orientations uniformly and independently distributed over $(0, 1)$ and $\{\pm 1\}$, respectively, because of the effect of geometrical spreading. It can be shown that $F_C(\theta; w)$ and $F_T(\theta; w)$ respectively represent the probabilities that a ray chosen at random from the ray tube crosses the junction, or turns and exits by the North or South exits. (29) and (30) state that the power flows out of the junction can be found by integrating the probability densities $F_C(\theta; w)$ and $F_T(\theta; w)$ with respect to the ray angle θ, after multiplication by the appropriate absorption factor.

4.4. Other junctions

The integral approximation procedure of §4.1 can be used to calculate acoustic power flows at junctions other than crossroads. For example, in the 'side street' geometry of Figure 4(b), for $l \gg 1$ and $\alpha \ll 1$ we can approximate

$$P^E \sim \frac{1}{\pi} \int_0^{\pi/2} (1-\alpha)^{l \tan\theta} F_C(\theta; w/2)\, d\theta, \qquad P^N \sim \frac{2}{\pi} \int_0^{\pi/2} (1-\alpha)^{l \tan\theta} F_T(\theta; w/2)\, d\theta.$$

Note that the power loss to a single side street of width w is exactly the same as the combined losses to the two side streets at a crossroads where the ratio between the main and crossing streets is $w/2$. This result is completely intuitive when one considers the geometrical correspondence between these two junction types: reflecting the single side street in the lower wall produces a crossroads with the same side street width w but with a main street width of 2.

Such reflection arguments can be used to predict the energy redistribution at other junction types. For example, for the 'T-junction' geometry of Figure 4(c), reflection in the far-right wall produces

a crossroads of side street width $2w$, so that

$$P^W \sim \frac{1}{\pi}\int_0^{\pi/2}(1-\alpha)^{l\tan\theta}F_C(\theta;2w)\,d\theta, \qquad P^N \sim P^S \sim \frac{1}{\pi}\int_0^{\pi/2}(1-\alpha)^{l\tan\theta}F_T(\theta;2w)\,d\theta,$$

where P^W should be interpreted as the power flow back down the main street due to reflection off the far wall. Power flows in the 'right-angled bend' geometry of Figure 4(d) can be treated similarly.

Asymmetric junctions such as those in Figures 4(e) and 4(f) can also be considered. Although such geometries cannot be treated by a reflection argument, we can appeal to the probabilistic interpretation of §4.3. We first consider the case depicted in Figure 4(e), where $w_2 > 1$. Assuming that the offset and orientation of a ray incident on the junction are random, uniform and independent, the probability that a ray crosses the junction and leaves by the East exit is

$$\tilde{F}_C(\theta;w_1,w_2) = \begin{cases} 1, & 0<\theta<\theta_*^-, \\ \frac{w_2+1}{2} - w_1\tan\theta, & \theta_*^-<\theta<\theta_*^+, \\ 0, & \theta_*^+<\theta<\pi/2, \end{cases} \tag{31}$$

where

$$\theta_*^- = \arctan\frac{w_2-1}{2w_1}, \qquad \theta_*^+ = \arctan\frac{w_2+1}{2w_1}.$$

The probability that the ray leaves by the North exit is equal to the probability that it leaves by the South exit, namely

$$\tilde{F}_T(\theta;w_1,w_2) = \begin{cases} 0, & 0<\theta<\theta_*^-, \\ \frac{w_1\tan\theta}{2} - \frac{w_2-1}{2}, & \theta_*^-<\theta<\theta_*^+, \\ \frac{1}{2}, & \theta_*^+<\theta<\pi/2. \end{cases} \tag{32}$$

We therefore propose the approximations

$$P^E \sim \frac{1}{\pi}\int_0^{\pi/2}(1-\alpha)^{l\tan\theta}\tilde{F}_C(\theta;w_1,w_2)\,d\theta, \qquad P^N \sim P^S \sim \frac{1}{\pi}\int_0^{\pi/2}(1-\alpha)^{l\tan\theta}\tilde{F}_T(\theta;w_1,w_2)\,d\theta. \tag{33}$$

In the case of Figure 4(f), where $w_2 < 1$, the approximations (33) still hold, but now with

$$\tilde{F}_C(\theta;w_1,w_2) = \begin{cases} w_2, & 0<\theta<\theta_*^-, \\ \frac{w_2+1}{2} - w_1\tan\theta, & \theta_*^-<\theta<\theta_*^+, \\ 0, & \theta_*^+<\theta<\pi/2, \end{cases}$$

$$\tilde{F}_T(\theta;w_1,w_2) = \begin{cases} 2w_1\tan\theta & 0<\theta<\theta_*^- \\ \frac{w_1\tan\theta}{2} - \frac{w_2-1}{4} & \theta_*^-<\theta<\theta_*^+ \\ \frac{1}{2} & \theta_*^+<\theta<\pi/2, \end{cases}$$

where now $\theta_*^- = \arctan\left((1-w_2)/(2w_1)\right)$. There is now the further possibility that rays are reflected back down the main street towards the source. This occurs with probability

$$\tilde{F}_B(\theta;w_1,w_2) = \begin{cases} 1-w_2-2w_1\tan\theta, & 0<\theta<\theta_*^-, \\ 0, & \theta_*^-<\theta<\theta_*^+, \\ 0, & \theta_*^+<\theta<\pi/2, \end{cases}$$

and we then have

$$P^W \sim \frac{1}{\pi}\int_0^{\pi/2} (1-\alpha)^{l\tan\theta}\tilde{F}_B(\theta; w_1, w_2)\, d\theta.$$

To end this section, we remark that this probabilistic approach could, in principle, be applied to the study of a much more general class of junctions than those presented here. For example, it should be possible to remove the requirement that intersecting streets meet at right angles.

5. Multiple junctions in 2D

We now show how the acoustic power flows in domains involving more than one junction can be computed using the ray tube model.

5.1. Energy redistribution at a second junction in 2D

We begin by considering the two-junction domain illustrated in Figure 8(a). According to the ray tube model, the power flow $P^E(2)$ out of the East exit of the second crossroads is

$$P^E(2) = \frac{1}{2\pi}\sum_{n\in\mathbb{Z}} (1-\alpha)^{|n|}\Theta_n, \tag{34}$$

where α is the absorption coefficient of the main street and $\Theta_n = \Theta_n(l_0, l_1, w_1, w_2, y_0)$ is the sum of the angular widths of the ray tubes from the nth image source in (10) that are incident on the East exit (in general there may be up to two such ray tubes).

The summation of (34) is slightly easier when we transform to the image street representation

$$P^E(2) = \frac{1}{2\pi}\sum_{n\in\mathbb{Z}} (1-\alpha)^{|n|}\tilde{\Theta}_n, \tag{35}$$

where $\tilde{\Theta}$, defined as in (14), is the contribution from the nth image street cross-section. To compute $\tilde{\Theta}_n$ for a given n we must determine the sum of the angular widths of the ray tubes from the source that are incident on the nth image street cross-section. These ray tubes are found by taking the ray tube that would be incident on the nth image street cross-section if the first junction were *not* present and removing those rays which intersect any of the images of the side street entrances of the first junction. A illustration of some of the resulting ray tubes for the geometry in Figure 8(a) is shown in Figure 8(b). This algorithmic method of calculating $\tilde{\Theta}_n$ is easily implemented on a computer, and the sum (35) can therefore be evaluated numerically. However, a simple closed-form analytical expression for $\tilde{\Theta}_n$ equivalent to the algorithmic calculation does not seem to exist.

In the single junction case it was found that when $l_0 \gg 1$ and $\alpha \ll 1$ the ray tube sum could be approximated by an integral over power densities propagating at each ray angle θ. We now proceed by assuming that the same is true in the two junction case when $l_0, l_1 \gg 1$ and $\alpha \ll 1$, and the integral approximation we propose is

$$P^E_{\text{app}}(2) = \frac{1}{\pi}\int_0^{\pi/2} (1-\alpha)^{l_0\tan\theta} F_C(\theta; w_1)(1-\alpha)^{l_1\tan\theta} F_C(\theta; w_2)\, d\theta. \tag{36}$$

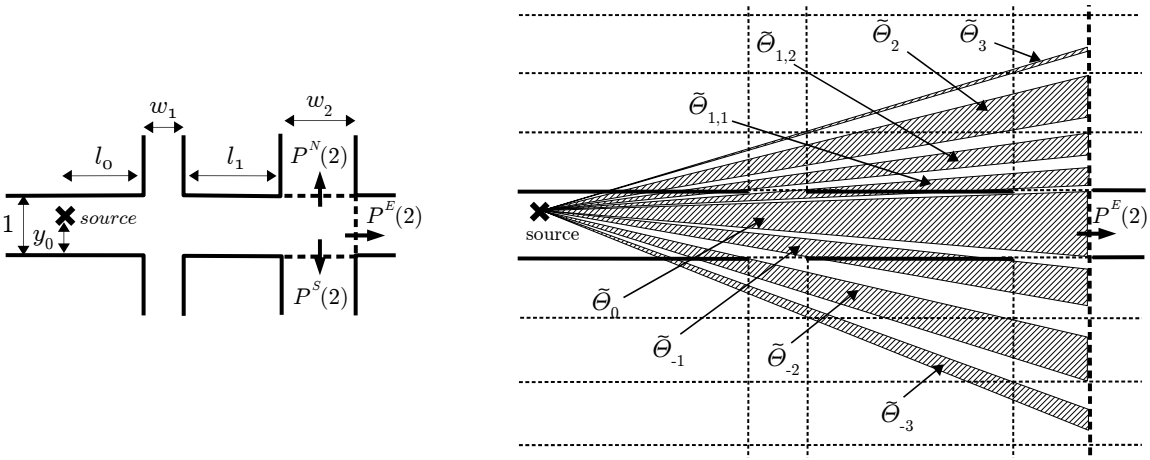

(a) Problem geometry (b) A portion of the ray tube diagram for $P^E(2)$

Figure 8: Energy redistribution at a second crossroads

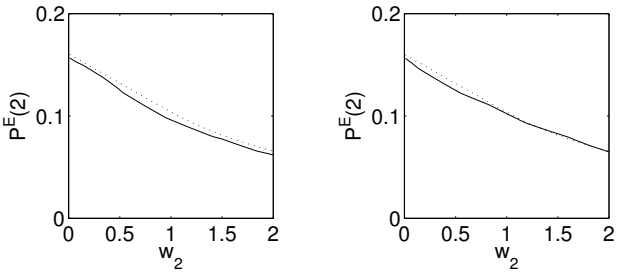

(a) $l_0 = 2$, $l_1 = 2$ (b) $l_0 = 2$, $l_1 = 2.4$

Figure 9: Comparison of (35) (solid line) and (36) (dotted line), with $y_0 = 0.4$, $w_1 = 0.8$, $\alpha = 0.02$.

Comparing (36) with (29), we note that the extra factors $(1-\alpha)^{l_1 \tan\theta}$ and $F_C(\theta; w_2)$ in the integrand in (36) represent the effects of wall absorption in the second street and energy redistribution at the second junction, respectively.

5.2. Validity of integral approximation: expected power flows

Numerical experiments do indeed validate (36) as a good approximation to (35), even for values of l_0 and l_1 as small as 2, as Figure 9 demonstrates. However, the lack of a convenient analytical expression for $\tilde{\Theta}_n$ makes it difficult to determine whether (36) is truly an asymptotic approximation to (35) in the joint limit $l_0, l_1 \gg 1$ with $\alpha \ll 1$. In this section we investigate this question by means of numerical experiments, and make a conjecture about the sense in which the approximation holds.

The accuracy of the integral approximation (36) depends in a rather complicated way on the ratio between the street lengths l_0 and l_1. In Figure 10 we plot the error $R = P^E_{\text{app}}(2) - P^E(2)$ as a function of the ratio $\lambda = l_0/l_1$, for two different values of l_0, and all other parameters fixed. For both values of l_0 the maximum error is about 0.005, with peaked oscillations occuring near the points $\lambda = 1, 1/2, 3/2, 2/3, 4/3$. In fact, such oscillations can be observed on a smaller scale around any rational value of λ, although the amplitude of the peaks seems to decrease as the denominator

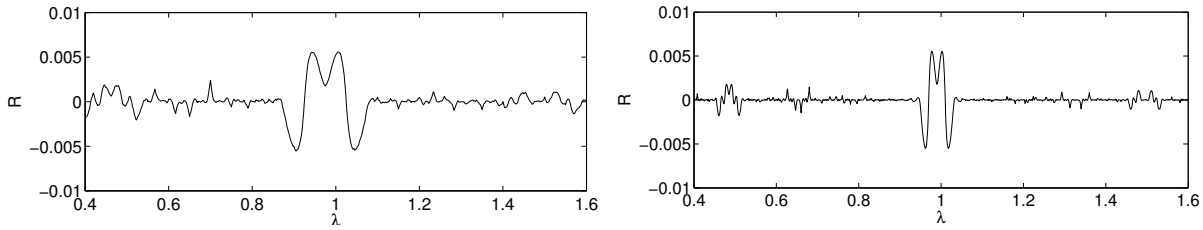

(a) $l_0 = 20$ (b) $l_0 = 100$

Figure 10: Plot of the error $R = P^E_{\text{app}}(2) - P^E(2)$ as a function of $\lambda = l_0/l_1$, with $y_0 = 0.5$, $w_1 = 1$, $w_2 = 1$, $\alpha = 0$.

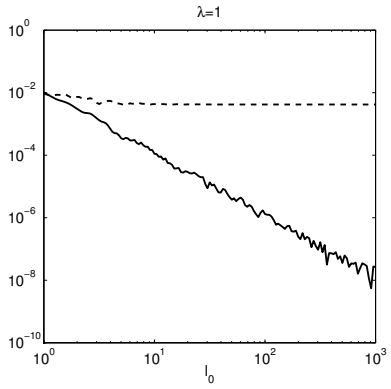

Figure 11: Logarithmic plot of $|\langle R\rangle|$ (solid line) and $|R|$ (dashed line) as a function of l_0 for $\lambda = 1$, $\lambda' = \frac{1}{\sqrt{l_0}}$ and parameter values $y_0 = 0.4$, $w_1 = 0.8$, $w_2 = 1$, $\alpha = 0$.

in the fractional representation of λ increases. Also, further numerical experiments suggest that the oscillations persist even for very large l_0. It would therefore seem that the convergence is not uniform in λ.

One way to deal with such difficulties is to weaken the notion of convergence required. Suppose we consider a local average of $P^E(2)$ in the vicinity of λ, defining

$$\left\langle P^E(2)\right\rangle := \frac{1}{2\lambda'}\int_{\lambda-\lambda'}^{\lambda+\lambda'} P^E(2)(\tilde{\lambda})\,d\tilde{\lambda}, \tag{37}$$

for some $\lambda' > 0$. We might then conjecture that if λ' is chosen appropriately, the oscillations observed in $P^E(2)$ should average out in the limit as $l_0 \to \infty$, with the averaged behaviour being given by $P^E_{\text{app}}(2)$. Numerical experiments suggest that the oscillations in R have a typical wavelength of the order $1/l_0$, so we certainly need to choose $\lambda' \gg 1/l_0$. Figure 11 shows the average error $\langle R\rangle = P^E_{\text{app}}(2) - \left\langle P^E(2)\right\rangle$ in the case where $\lambda' = 1/\sqrt{l_0}$, alongside the unaveraged error R. The gradient of the solid line is found to be approximately 2, so that, in this case, it appears that $\langle R\rangle = O\left(1/l_0^2\right)$ as $l_0 \to \infty$.

We therefore conjecture that $P^E_{\text{app}}(2) \sim \left\langle P^E(2)\right\rangle$ as $l_0 \to \infty$, so that our integral approximation represents an *expected* power flow, in the sense of (37). In assessing this interpretation we need to remember our assumption that the street geometry may be known only to a certain degree of accuracy.

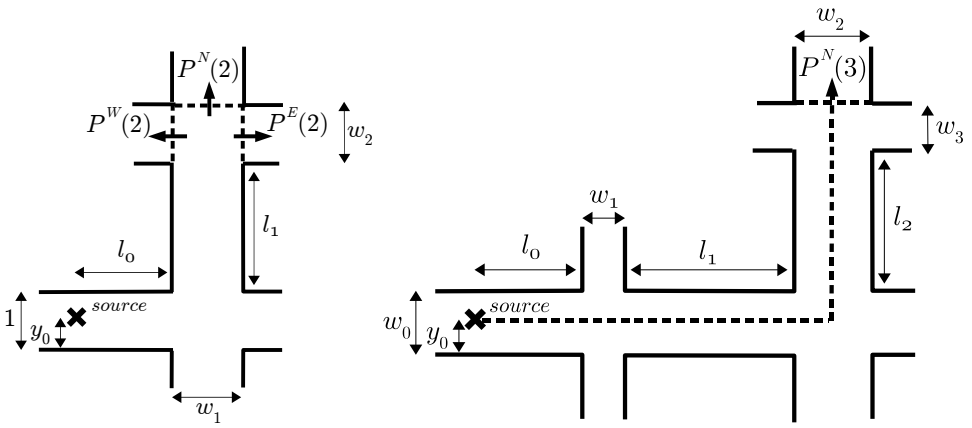

(a) Another two-junction geometry

(b) A three-junction geometry

Figure 12: Multiple-junction geometries

5.3. Further examples

The case where the absorption coefficient takes a value α_0 between the source and the first junction, and a different value α_1 between the first and second junctions, can be treated by modifying (36) to

$$P^E_{\text{app}}(2) = \frac{1}{\pi}\int_0^{\pi/2} (1-\alpha_0)^{l_0\tan\theta} F_C(\theta; w_1)\,(1-\alpha_1)^{l_1\tan\theta} F_C(\theta; w_2)\,d\theta. \tag{38}$$

Expected values of $P^N(2)$ and $P^S(2)$ can be obtained by replacing the factor of $F_C(\theta; w_2)$ in (38) by a factor of $F_T(\theta; w_2)$, so that

$$P^N_{\text{app}}(2) = P^S_{\text{app}}(2) = \frac{1}{\pi}\int_0^{\pi/2} (1-\alpha_0)^{l_0\tan\theta} F_C(\theta; w_1)\,(1-\alpha_1)^{l_1\tan\theta} F_T(\theta; w_2)\,d\theta.$$

In Figure 12(a) we consider another two-junction geometry. The integral approximations we propose for the expected power flows out of the second junction are

$$P^N_{\text{app}}(2) = \frac{1}{\pi}\int_0^{\pi/2} (1-\alpha_0)^{l_0\tan\theta} F_T(\theta; w_1)\,(1-\alpha_1)^{\frac{l_1}{w_1}\tan(\pi/2-\theta)} F_C\left(\pi/2-\theta; \frac{w_2}{w_1}\right) d\theta, \tag{39}$$

$$P^E_{\text{app}}(2) = P^W_{\text{app}}(2) = \frac{1}{\pi}\int_0^{\pi/2} (1-\alpha_0)^{l_0\tan\theta} F_T(\theta; w_1)\,(1-\alpha_1)^{\frac{l_1}{w_1}\tan(\pi/2-\theta)} F_T\left(\pi/2-\theta; \frac{w_2}{w_1}\right) d\theta. \tag{40}$$

The replacement of θ by $\pi/2-\theta$ in the factors for the second street is necessary because of the change of orientation from an East-West street to a North-South street after turning at the first junction.

5.4. More than two junctions

Integral approximations for the expected power flows in domains involving more than two junctions can be constructed similarly. For example, consider the path shown in Figure 12(b). For generality, the street width w_0 is assumed to be of the same order of magnitude, but not the exactly equal to, the characteristic lengthscale L used in the nondimensionalisation. We then approximate $P^N(3)$ by

$$P^N_{\rm app}(3) = \frac{1}{\pi}\int_0^{\pi/2} (1-\alpha_0)^{\frac{l_0}{w_0}\tan\theta} F_C\left(\theta; \frac{w_1}{w_0}\right) (1-\alpha_1)^{\frac{l_1}{w_0}\tan\theta} F_T\left(\theta; \frac{w_2}{w_0}\right) \times (1-\alpha_2)^{\frac{l_2}{w_2}\tan(\pi/2-\theta)} F_C\left(\pi/2-\theta; \frac{w_3}{w_2}\right) d\theta.$$

Since $F_C(\theta; w_1/w_0)$ vanishes for $\theta \geq \arctan(w_0/w_1)$, and $F_R(\pi/2-\theta; w_3/w_2)$ vanishes for $\theta \leq \arctan(w_3/w_2)$, we find that if $w_3/w_2 \geq w_0/w_1$ then the expected power flow is zero, since the integrand vanishes completely on the range $(0, \pi/2)$.

This example illustrates a more general result. Suppose that an arbitrary path through a network of streets crosses a junction in the East-West direction, with the ratio between the widths of the 'side street' and the 'main street' given by R_{EW}, and that this path also crosses a junction in the North-South direction, with the ratio between the widths of the 'side street' and the 'main street' given by R_{NS}. Then if $R_{EW}R_{NS} \geq 1$, the expected power flow along the path is zero. In particular, in the special case where the street widths are all equal, there is no expected power flow along any path which crosses junctions in both the East-West and North-South directions.

6. A network of streets in 2D

We now apply the ideas developed in §3-5 to estimate the power flows in an infinite rectangular network of streets intersecting at right-angled crossroads. Indexing the crossroads by $(x, y) \in \mathbb{Z}\times\mathbb{Z}$, we let $l^S_{x,y}, w^S_{x,y}, \alpha^S_{x,y}$ and $l^W_{x,y}, w^W_{x,y}, \alpha^W_{x,y}$ denote the lengths, widths and absorption coefficients of the streets to the South and West respectively of junction (x, y). We assume that the source lies in the street between junctions $(0, 0)$ and $(1, 0)$, a distance d_0 from the junction $(1, 0)$.

The net power flows $P^N_{x,y}$, $P^E_{x,y}$, $P^S_{x,y}$ and $P^W_{x,y}$ out of a junction (x, y) are made up of contributions from the infinitely many propagation paths that exist between the source and that junction. The expected power flow along any particular path can be estimated by the integral approximation method developed in §3-5, provided that the street lengths are much larger than the street widths, and that the absorption coefficients are small. Some paths make a positive contribution to the power flow, and others make a negative one, depending on the direction in which the energy is propagating when it crosses the junction exit in question. Some paths make no contribution at all, as remarked in §5.4. Classifying all of these paths and explicitly summing their respective contributions might appear to be rather difficult, but in §6.2 we show how this can be achieved by reformulating the problem as a coupled system of partial difference equations. Before describing this model, we first show how an approximation to the net power flows can be obtained by considering a subset of paths which make the largest contribution. To demonstrate this, we consider the special case of a *regular* network in which $l^S_{x,y} = l^W_{x,y} = l$, $w^S_{x,y} = w^W_{x,y} = w$ and $\alpha^S_{x,y} = \alpha^W_{x,y} = \alpha$ for all (x, y), where l, w and α are constant. Furthermore we assume, without loss of generality, that $x \geq 1$ and $y \geq 0$, and study the net power flow $P^E_{x,y}$ out of the East exit of the junction (x, y).

6.1. Paths of minimal length

Since the power flow along any path through the network decreases with each junction encountered, a reasonable estimate of $P^E_{x,y}$ can be obtained by considering only those paths that have *minimal length*, in the sense that they encounter exactly $x+y$ junctions. The number of such paths is equal to $\binom{x+y-1}{x-1}$ (see [10, Appendix B]). However, only a subset of these paths make a non-zero contribution to the net power flow, since there is no propagation along any path that crosses junctions in both the West-East and South-North directions (recall §5.4). The number $M_{x,y}$ of paths of minimal length that do contribute is [10, Appendix B]

$$M_{x,y} = \begin{cases} \binom{x}{y}, & x \geq y \\ \binom{y-1}{x-1}, & x < y. \end{cases}$$

Each of these paths makes the *same* contribution to the power flow, namely

$$P^{E,\text{path}}_{x,y} = \frac{1}{\pi} \int_0^{\pi/2} \beta^{(x-d_0/l)\tan\theta + y\tan(\pi/2-\theta)} f(\theta)\, d\theta,$$

where $\beta = (1-\alpha)^{l/w}$ and

$$f(\theta) = \begin{cases} F_C(\theta,1)^{x-y} F_T(\theta,1)^y F_T(\pi/2-\theta,1)^y, & x \geq y, \\ F_C(\pi/2-\theta,1)^{y-x} F_T(\theta,1)^x F_T(\pi/2-\theta,1)^x, & x < y. \end{cases}$$

Our estimate for the net power flow $P^E_{x,y}$ is then

$$P^E_{x,y} = M_{x,y} P^{E,\text{path}}_{x,y}. \tag{41}$$

Plots of (41) for two different values of β can be found in Figure 13(a)-(b). These plots suggest that the power flow decays *exponentially* with increasing distance from the source, with the fastest decay rate being along the diagonal $x = y$. This can be verified by direct analysis of (41), as we now show. For ease of presentation we consider the case where $\alpha = 0$ (so that $\beta = 1$). Setting $N = x + y$, $\lambda = y/N = 1 - x/N$ and

$$\begin{aligned} P^E_\lambda(N) := P^E_{x,y} &= P^E_{(1-\lambda)N,\lambda N}, \\ P^{E,\text{path}}_\lambda(N) := P^{E,\text{path}}_{x,y} &= P^{E,\text{path}}_{(1-\lambda)N,\lambda N}, \\ M_\lambda(N) := M_{x,y} &= M_{(1-\lambda)N,\lambda N}, \end{aligned}$$

equation (41) becomes

$$P^E_\lambda(N) = M_\lambda(N) P^{E,\text{path}}_\lambda(N). \tag{42}$$

We now investigate the behaviour of $P^E_\lambda(N)$ for N large and $0 \leq \lambda < 1$ fixed.

- When $\lambda = 0$ we have $M_0(N) = 1$ and our estimate for $P^E_0(N)$ is

$$P^E_0(N) = \frac{1}{\pi} \int_0^{\pi/2} F_C(\theta;1)^N\, d\theta = \frac{1}{\pi} \int_0^{\pi/4} \exp\left[N \log\left(1 - \tan\theta\right)\right] d\theta, \tag{43}$$

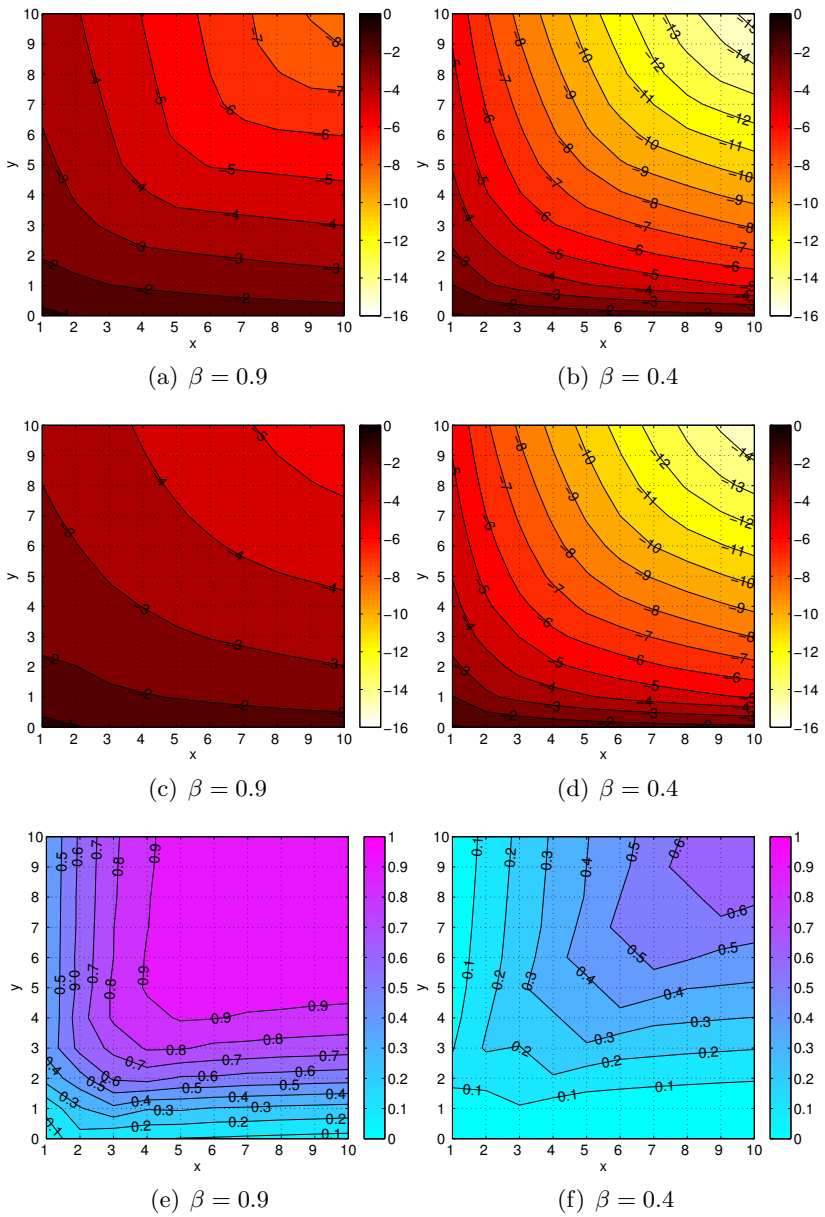

(a) $\beta = 0.9$ (b) $\beta = 0.4$

(c) $\beta = 0.9$ (d) $\beta = 0.4$

(e) $\beta = 0.9$ (f) $\beta = 0.4$

Figure 13: (a)-(b) Contour plots of $\log_{10} P^E_{x,y}$ for two different values of β, computed by (41) (i.e. using only paths of minimal length). (c)-(d) Corresponding plots of $\log_{10} P^E_{x,y}$, computed by (52) (i.e. by solving the full partial difference equation model). (e)-(f) Relative error between the two.

which is a Laplace-type integral with large parameter N. The main contribution to (43) comes from the left endpoint $\theta = 0$, and a local expansion around this point reveals that

$$P_0^E(N) \sim \frac{1}{N\pi}, \qquad N \to \infty, \tag{44}$$

so that the decay is *algebraic* in the number of junctions encountered.

- Along the diagonal $\lambda = 1/2$ (with N even) there is again only one contributing path of minimal

length ($M_{1/2}(N) = 1$ for all N even) and our estimate for $P^E_{1/2}(N)$ is

$$P^E_{1/2}(N) = \frac{1}{\pi}\int_0^{\pi/2} F_T\left(\theta;1\right)^{N/2} F_T\left(\pi/2-\theta;1\right)^{N/2}\, d\theta = \frac{2}{\pi}\int_0^{\pi/4} \exp\left[N\left(\frac{1}{2}\log\left(\frac{\tan\theta}{4}\right)\right)\right] d\theta,$$

where we have used the symmetry of the integrand to reduce the range of integration to $\theta \in (0, \pi/4)$. Again, this is a Laplace-type integral, although this time the main contribution comes from the right endpoint $\theta = \pi/4$, with

$$P^E_{1/2}(N) \sim \frac{2}{N\pi}\left(\frac{1}{2}\right)^N, \quad N \to \infty,\ N \text{ even}, \tag{45}$$

so that the decay is *exponential* in the number of junctions encountered.

- In the intermediate case $0 < \lambda < 1/2$, we first note that by Stirling's approximation,

$$M_\lambda(N) = \frac{((1-\lambda)N)!}{(\lambda N)!((1-2\lambda)N)!} \sim \sqrt{\frac{(1-\lambda)}{2\pi N\lambda(1-2\lambda)}}\left(\left(\frac{(1-2\lambda)^2}{\lambda(1-\lambda)}\right)^\lambda\left(\frac{1-\lambda}{1-2\lambda}\right)\right)^N, \quad N\to\infty. \tag{46}$$

Along each of the contributing paths we have

$$\begin{aligned} P^{E,\text{path}}_\lambda(N) &= \frac{1}{\pi}\int_0^{\pi/2} F_T(\theta;1)^{\lambda N} F_T(\pi/2-\theta;1)^{\lambda N} F_C(\theta;1)^{(1-2\lambda)N}\, d\theta \\ &= \frac{1}{\pi}\int_0^{\pi/4} \exp\left[N\left(\lambda\log\left(\frac{\tan\theta}{4}\right) + (1-2\lambda)\log\left(1-\tan\theta\right)\right)\right] d\theta, \end{aligned}$$

since $F_C(\theta;1) = 0$ for $\theta > \pi/4$. The main contribution now comes from the interior point $\theta = \arctan\left(\lambda/(1-\lambda)\right)$, and we find that

$$P^{E,\text{path}}_\lambda(N) \sim \frac{1}{\pi}\sqrt{\frac{2}{N}}\frac{\sqrt{(1-2\lambda)(1-\lambda)\lambda}}{(1-\lambda)^2+\lambda^2}\left(\left(\frac{\lambda(1-\lambda)}{4(1-2\lambda)^2}\right)^\lambda\left(\frac{1-2\lambda}{1-\lambda}\right)\right)^N, \quad N\to\infty. \tag{47}$$

Combining (46) and (47), we conclude that (42) has the asymptotic behaviour

$$P^E_\lambda(N) \sim \frac{1}{N\pi}\left(\frac{1-\lambda}{(1-\lambda)^2+\lambda^2}\right)\left(\frac{1}{2}\right)^{2\lambda N}, \quad N\to\infty. \tag{48}$$

- Finally, when $1/2 < \lambda < 1$ a similar analysis reveals that

$$P^E_\lambda(N) \sim \frac{1}{N\pi}\left(\frac{\lambda}{(1-\lambda)^2+\lambda^2}\right)\left(\frac{1}{2}\right)^{2(1-\lambda)N}, \quad N\to\infty. \tag{49}$$

We therefore conclude that the power flow decays exponentially in N for all $0 < \lambda < 1$, with the maximum decay rate occurring along the diagonal $\lambda = 1/2$. Note that setting $\lambda = 0$ in expression (48) returns the algebraic decay predicted by (44). However, with $\lambda = 1/2$ (and N even), both (48) and (49) return precisely $1/2$ times the prediction of (45). This is because in the cases $0 < \lambda < 1/2$ and $1/2 < \lambda < 1$ energy propagates only along rays with launch angles in the ranges $\theta \in (0, \pi/4)$ and $\theta \in (\pi/4, \pi/2)$, respectively, whereas in the special case $\lambda = 1/2$ energy propagates along rays of all angles $\theta \in (0, \pi/2)$. The correct behaviour for $\lambda = 1/2$ can therefore only be recovered by considering the *sum* of the limiting values of (48) and (49) as $\lambda \to 1/2$ from below and above:

$$P^E_{1/2}(N) \sim P^E_{1/2-}(N) + P^E_{1/2+}(N), \quad N\to\infty.$$

6.2. Partial difference equation model

So far we have considered only the contribution from paths of minimal length. We now generalise our model to take into account the contribution of *all* the propagation paths through the network. At each junction in the lattice we define $p^N_{x,y}(\theta)$, $p^E_{x,y}(\theta)$, $p^S_{x,y}(\theta)$, $p^W_{x,y}(\theta)$ to be the θ-resolved power flows out of the junction (x, y) in the North, East, South and West directions, respectively. We can use the energy redistribution and absorption rules suggested by the integral approximations developed in previous sections to write down a coupled system of partial difference equations satisfied by these quantities. For example, the power flow $p^N_{x,y}(\theta)$ out of the North exit is a sum of contributions flowing in from the East, South and West streets, each involving an appropriate choice of the redistribution functions F_C and F_T. The resulting system of partial difference equations, for the case of a general network of streets, is

$$\begin{aligned}
p^N_{x,y} &= F_C\left(\pi/2-\theta;\tfrac{w^W_{x,y}}{w^S_{x,y}}\right)(\beta^N_{x,y-1})^{1/t}p^N_{x,y-1} + F_T\left(\theta;\tfrac{w^S_{x,y}}{w^W_{x,y}}\right)\left((\beta^E_{x-1,y})^t p^E_{x-1,y} + (\beta^W_{x+1,y})^t p^W_{x+1,y}\right) + \Phi^N_{x,y},\\
p^E_{x,y} &= F_C\left(\theta;\tfrac{w^S_{x,y}}{w^W_{x,y}}\right)(\beta^E_{x-1,y})^t p^E_{x-1,y} + F_T\left(\pi/2-\theta;\tfrac{w^W_{x,y}}{w^S_{x,y}}\right)\left((\beta^N_{x,y-1})^{1/t}p^N_{x,y-1} + (\beta^S_{x,y+1})^{1/t}p^S_{x,y+1}\right) + \Phi^E_{x,y},\\
p^S_{x,y} &= F_C\left(\pi/2-\theta;\tfrac{w^W_{x,y}}{w^S_{x,y}}\right)(\beta^S_{x,y+1})^{1/t}p^S_{x,y+1} + F_T\left(\theta;\tfrac{w^S_{x,y}}{w^W_{x,y}}\right)\left((\beta^E_{x-1,y})^t p^E_{x-1,y} + (\beta^W_{x+1,y})^t p^W_{x+1,y}\right) + \Phi^S_{x,y},\\
p^W_{x,y} &= F_C\left(\theta;\tfrac{w^S_{x,y}}{w^W_{x,y}}\right)(\beta^W_{x+1,y})^t p^W_{x+1,y} + F_T\left(\pi/2-\theta;\tfrac{w^W_{x,y}}{w^S_{x,y}}\right)\left((\beta^N_{x,y-1})^{1/t}p^N_{x,y-1} + (\beta^S_{x,y+1})^{1/t}p^S_{x,y+1}\right) + \Phi^W_{x,y},
\end{aligned} \tag{50}$$

where $t = \tan\theta$,

$$\begin{aligned}
\beta^S_{x,y} &= (1-\alpha^S_{x,y})^{\frac{l^S_{x,y}}{w^S_{x,y}}}, & \beta^W_{x,y} &= (1-\alpha^W_{x,y})^{\frac{l^W_{x,y}}{w^W_{x,y}}},\\
\beta^N_{x,y} &= \beta^S_{x,y+1}, & \beta^E_{x,y} &= \beta^W_{x+1,y},
\end{aligned}$$

and Φ^N, Φ^E Φ^S and Φ^W are source terms to be specified according to the distribution of sources in the network. For example, in the case where the source lies in the street between junctions $(0, 0)$ and $(1, 0)$, the appropriate source functions are zero everywhere except for

$$\begin{aligned}
\Phi^N_{0,0} = \Phi^S_{0,0} &= \left(\beta^W_{1,0}\right)^{\frac{\left(l^W_{1,0}-d\right)t}{l^W_{1,0}}} F_T\left(\theta,\tfrac{w^S_{0,0}}{w^W_{1,0}}\right), & \Phi^W_{0,0} &= \left(\beta^W_{1,0}\right)^{\frac{\left(l^W_{1,0}-d\right)t}{l^W_{1,0}}} F_C\left(\theta,\tfrac{w^S_{0,0}}{w^W_{1,0}}\right),\\
\Phi^N_{1,0} = \Phi^S_{1,0} &= \left(\beta^W_{1,0}\right)^{\frac{d}{l^W_{1,0}}t} F_T\left(\theta,\tfrac{w^S_{1,0}}{w^W_{1,0}}\right), & \Phi^E_{1,0} &= \left(\beta^W_{1,0}\right)^{\frac{d}{l^W_{1,0}}t} F_C\left(\theta,\tfrac{w^S_{1,0}}{w^W_{1,0}}\right),
\end{aligned} \tag{51}$$

where d is the distance from the source to the junction $(1, 0)$.

6.3. Calculation of net power flows and mean-square pressures

If the system (50) can be solved for each $\theta \in (0, \pi/2)$, net power flows can be found by integrating appropriate combinations of the solutions over θ. For example, the net power flow $P^E_{x,y}$ out of the East exit of the junction (x, y) is

$$P^E_{x,y} = \int_0^{\pi/2} p^E_{x,y}(\theta) - \left(\beta^W_{x+1,y}\right)^t p^W_{x+1,y}(\theta)\, d\theta. \tag{52}$$

Furthermore, knowledge of the θ-resolved power densities also allows us to calculate the average value of the acoustic energy density over a street cross-section. For example, the average energy density over the cross-section halfway between junctions (x, y) and $(x + 1, y)$ is proportional to

$$W^E_{x,y} = \frac{1}{w^W_{x+1,y}} \int_0^{\pi/2} \frac{\left(\beta^W_{x+1,y}\right)^{t/2} \left(p^E_{x,y}(\theta) + p^W_{x+1,y}(\theta)\right)}{\cos\theta}\, d\theta. \tag{53}$$

Recalling the discussion in §2, (53) is also proportional to the average value of the mean-square pressure over the same street cross-section.

6.4. Exact solution in a regular network

The system (50) is difficult to solve analytically. However, in the special case of a regular network the system decouples and an analytical solution can be found, as we now demonstrate. The equations have different forms depending on whether $\theta < \pi/4$ or $\theta > \pi/4$, and we first consider the case $0 < \theta < \pi/4$. For notational convenience we introduce the shift operators X, Y defined on a quantity $f_{x,y}$ by

$$(Xf)_{x,y} = f_{x+1,y}, \qquad (Yf)_{x,y} = f_{x,y+1}.$$

In this notation the system (50) becomes

$$\begin{aligned} p^N &= \tfrac{t}{2}\beta^t(X^{-1}p^E + Xp^W) + \Phi^N, & p^E &= (1-t)\beta^t X^{-1}p^E + \tfrac{1}{2}\beta^{1/t}(Y^{-1}p^N + Yp^S) + \Phi^E, \\ p^S &= \tfrac{t}{2}\beta^t(X^{-1}p^E + Xp^W) + \Phi^S, & p^W &= (1-t)\beta^t Xp^W + \tfrac{1}{2}\beta^{1/t}(Y^{-1}p^N + Yp^S) + \Phi^W, \end{aligned} \tag{54}$$

and by eliminating p^E, p^S and p^W from (54) we may obtain a single partial difference equation for p^N of the form

$$L[p^N] = \psi, \tag{55}$$

where, with $\rho := (1-t)\beta^t$,

$$\begin{aligned} L &:= \frac{\beta^{1/t}}{4}\left(X + X^{-1} - 2\rho\right)\left(Y + Y^{-1}\right) + \frac{(1-t)}{t}\left(X + X^{-1} - (\rho^{-1} + \rho)\right), \\ \psi &:= -\frac{\beta^{1/t}}{4}\left(X + X^{-1} - 2\rho\right) Y\left(\Phi^S - \Phi^N\right) - \frac{1}{2}\left(\left(X^{-1} - \rho\right)\Phi^E + (X - \rho)\Phi^W\right) \\ &\qquad + \frac{(1-t)}{t}\left(X + X^{-1} - (\rho^{-1} + \rho)\right)\Phi^N. \end{aligned}$$

In this case the source functions (51) are

$$\begin{aligned} \Phi^N_{0,0} &= \Phi^S_{0,0} = \beta^{\frac{(l-d)t}{l}}\left(\frac{t}{2\pi}\right), & \Phi^W_{0,0} &= \beta^{\frac{(l-d)t}{l}}\left(\frac{1-t}{\pi}\right), \\ \Phi^N_{1,0} &= \Phi^S_{1,0} = \beta^{\frac{dt}{l}}\left(\frac{t}{2\pi}\right), & \Phi^E_{1,0} &= \beta^{\frac{dt}{l}}\left(\frac{1-t}{\pi}\right), \end{aligned}$$

and ψ is found to be zero everywhere except for

$$\psi_{0,0} = \frac{1}{2\pi}\left(\beta^{\frac{dt}{l}}(1-t) - \beta^{-\frac{dt}{l}}\right), \qquad \psi_{1,0} = \frac{1}{2\pi}\left(\beta^{\frac{(l-d)t}{l}}(1-t) - \beta^{-\frac{(l-d)t}{l}}\right).$$

To solve (55) we first note that by analogy to the theory of linear partial differential equations with constant coefficients, if we can find a 'fundamental solution' $G_{x,y}$ satisfying the equation

$$L[G_{x,y}] = \delta_{x,y}, \tag{56}$$

where

$$\delta_{x,y} = \begin{cases} 1, & (x,y) = (0,0), \\ 0, & \text{otherwise}, \end{cases}$$

then a formal solution of the original problem (55) is provided by the convolution

$$p^N_{x,y} = (\psi * G)_{x,y} := \sum_{i,j} \psi_{i,j} X^{-i} Y^{-j} G_{x,y}. \tag{57}$$

Equation (56) can be solved by an application of the transform methods employed in [31, p. 365] and [32] to solve similar problems. We form the double Fourier series

$$F(\xi,\eta) := \sum_{x=-\infty}^{\infty} \sum_{y=-\infty}^{\infty} G_{x,y}\, \mathrm{e}^{\mathrm{i}(\xi x + \eta y)}, \tag{58}$$

and note that applying the translations X and Y to $G_{x,y}$ corresponds to multiplying $F(\xi,\eta)$ by $\mathrm{e}^{-\mathrm{i}\xi}$ and $\mathrm{e}^{-\mathrm{i}\eta}$, respectively. Under the transformation (58), equation (56) becomes

$$F(\xi,\eta) = \frac{1}{K(\xi,\eta)},$$

where

$$K(\xi,\eta) = \beta^{1/t}\left(\cos\xi - \rho\right)\cos\eta + \frac{(1-t)}{t}\left(2\cos\xi - (\rho^{-1} + \rho)\right).$$

A formal solution of (56) is then given by

$$G_{x,y} = \frac{1}{4\pi^2}\int_{-\pi}^{\pi}\int_{-\pi}^{\pi} \frac{\mathrm{e}^{-\mathrm{i}(\xi x + \eta y)}}{K(\xi,\eta)}\, d\xi d\eta = \frac{1}{\pi^2}\int_0^{\pi}\int_0^{\pi} \frac{\cos\xi x \cos\eta y}{K(\xi,\eta)}\, d\xi d\eta, \tag{59}$$

since $K(\xi,\eta)$ is even in both ξ and η. We remark that for $0 < t < 1$ and $0 < \beta < 1$, $K(\xi,\eta)$ is continuous and non-zero on $[0,\pi] \times [0,\pi]$, which guarantees convergence of the integral in (59) for all $(x,y) \in \mathbb{Z} \times \mathbb{Z}$. The integration over η in (59) can be carried out explicitly (see [10, Appendix C]) to give

$$G_{x,y} = -\frac{1}{\pi}\int_0^{\pi} \frac{c^{|y|}\cos\xi x}{\sqrt{b^2 - a^2}}\, d\xi, \tag{60}$$

where

$$a = \beta^{1/t}(\cos\xi - \rho), \qquad b = \frac{(1-t)}{t}\left(2\cos\xi - (\rho^{-1} + \rho)\right), \qquad c = -\frac{1}{a}\left(b + \sqrt{b^2 - a^2}\right).$$

With p^N determined by (57) and (60), the remaining variables p^E, p^S and p^W can be expressed in terms of p^N as follows:

$$p^S = p^N + (\Phi^S - \Phi^N), \tag{61}$$

$$p^E = \left[1 - \rho X^{-1}\right]^{-1} \left(\frac{\beta^{1/t}}{2} \left((Y + Y^{-1}) p^N + Y(\Phi^S - \Phi^N) \right) + \Phi^E \right), \tag{62}$$

$$p^W = \left[1 - \rho X\right]^{-1} \left(\frac{\beta^{1/t}}{2} \left((Y + Y^{-1}) p^N + Y(\Phi^S - \Phi^N) \right) + \Phi^W \right). \tag{63}$$

The inverse operators $\left[1 - \rho X^{\pm 1}\right]^{-1}$ in (62) and (63) are given formally by the sums

$$\left[1 - \rho X^{\pm 1}\right]^{-1} = \sum_{n=0}^{\infty} (\rho X^{\pm 1})^n, \tag{64}$$

which converge under fairly weak assumptions on p^N, Φ^N, Φ^E, Φ^S and Φ^W (e.g. boundedness), because $0 < \theta < \pi/4$ implies that $0 < \rho < 1$. In fact the action of (64) on p^N can be evaluated explicitly using the trigonometric identity

$$\sum_{n=0}^{\infty} \rho^n \cos \xi(x \pm n) = \frac{\cos \xi x - \rho \cos \xi(x \mp 1)}{1 + \rho^2 - 2\rho \cos \xi},$$

a proof of which is given in [10, Appendix C].

The solution of (54), valid for $0 < \theta < \pi/4$, can therefore be written as

$$\begin{array}{ll} p^N = \psi * G, & p^E = \psi * H^+ + S_1, \\ p^S = \psi * G + S_2, & p^W = \psi * H^- + S_3, \end{array} \tag{65}$$

where

$$H^{\pm}_{x,y} = -\frac{\beta^{1/t}}{2\pi} \int_0^{\pi} \frac{\left(\cos \xi x - \rho \cos \xi(x \pm 1)\right) \left(z^{|y+1|} + z^{|y-1|} \right)}{(1 + \rho^2 - 2\rho \cos \xi)\sqrt{b^2 - a^2}} \, d\xi,$$

and

$$\begin{aligned} S_1 &= \sum_{n=0}^{\infty} \left(\rho X^{-1}\right)^n \left(\frac{\beta^{1/t}}{2} Y(\Phi^S - \Phi^N) + \Phi^E \right), \\ S_2 &= \Phi^S - \Phi^N, \\ S_3 &= \sum_{n=0}^{\infty} (\rho X)^n \left(\frac{\beta^{1/t}}{2} Y(\Phi^S - \Phi^N) + \Phi^W \right). \end{aligned}$$

When $\pi/4 < \theta < \pi/2$, the system (54) is replaced by

$$\begin{array}{ll} p^N = \left(1 - \frac{1}{t}\right) \beta^{1/t} Y^{-1} p^N + \frac{1}{2} \beta^t \left(X^{-1} p^E + X p^W \right) + \Phi^N, & p^E = \frac{1}{2t} \beta^{1/t} \left(Y^{-1} p^N + Y p^S \right) + \Phi^E, \\ p^S = \left(1 - \frac{1}{t}\right) \beta^{1/t} Y p^S + \frac{1}{2} \beta^t \left(X^{-1} p^E + X p^W \right) + \Phi^S, & p^W = \frac{1}{2t} \beta^{1/t} \left(Y^{-1} p^N + Y p^S \right) + \Phi^W, \end{array} \tag{66}$$

and the source functions are zero everywhere except for

$$\Phi^N_{0,0} = \Phi^S_{0,0} = \beta^{\frac{(l-d)t}{l}} \left(\frac{1}{2\pi}\right), \qquad \Phi^N_{1,0} = \Phi^S_{1,0} = \beta^{\frac{dt}{l}} \left(\frac{1}{2\pi}\right). \tag{67}$$

Noting that (66) is simply (54) with

$$N \leftrightarrow E, \qquad S \leftrightarrow W, \qquad t \leftrightarrow 1/t, \qquad X \leftrightarrow Y, \tag{68}$$

the solution of (66), valid for $\pi/4 < \theta < \pi/2$, is found to be

$$\begin{array}{ll} p^N = \tilde{\psi} * \tilde{H}^+ + \tilde{S}_1, & p^E = \tilde{\psi} * \tilde{G}, \\ p^S = \tilde{\psi} * \tilde{H}^- + \tilde{S}_3, & p^W = \tilde{\psi} * \tilde{G} + \tilde{S}_2, \end{array} \tag{69}$$

where $\tilde{\psi}$ and $\tilde{S}_i$ are the previously defined expressions ψ and S_i under the transformations (68), and

$$\tilde{G}_{x,y} = G_{y,x}, \qquad \tilde{H}^{\pm}_{x,y} = H^{\pm}_{y,x},$$

under the transformation $t \leftrightarrow 1/t$. From (67) we find that $\tilde{\psi}$ is zero everywhere except for

$$\begin{array}{ll} \tilde{\psi}_{0,0} = -\frac{1-t}{2\pi t}\beta^{1/t+\frac{(l-d)t}{l}}, & \tilde{\psi}_{1,0} = -\frac{1-t}{2\pi t}\beta^{1/t+\frac{dt}{l}}, \\ \tilde{\psi}_{0,-1} = \tilde{\psi}_{0,1} = -\frac{1}{4\pi}\beta^{\frac{(l-d)t}{l}}, & \tilde{\psi}_{1,-1} = \tilde{\psi}_{1,1} = -\frac{1}{4\pi}\beta^{\frac{dt}{l}}. \end{array}$$

In Figure 13(c)-(d) we show logarithmic plots of the net power flow P^E defined by (52), computed using the solutions (65) and (69), for two different values of β. Comparing these to Figure 13(a)-(b) we note that the anisotropic decay predicted by the minimal length paths approach is clearly visible, although, as might have been expected, the minimal length path calculation underestimates the power flow derived via the full partial difference equation model. The relative error between (41) and (52) is plotted in Figure 13(e)-(f). Note that the relative error decreases as β decreases, so that the contribution of the non-minimal-length paths becomes less important as the amount of absorption increases.

As remarked in §6.3, knowledge of the power densities $p^N_{x,y}(\theta)$, $p^E_{x,y}(\theta)$, $p^S_{x,y}(\theta)$, $p^W_{x,y}(\theta)$ also allows us to estimate average energy densities and mean-square pressures. In Figure 14 we show logarithmic plots of the average energy density W^E defined by (53) for two different values of β.

6.5. The case $\beta = 1$ ($\alpha = 0$)

When $\beta = 1$ ($\alpha = 0$) the integral (59) is no longer convergent, and the θ-resolved power flows are no longer well-defined. However, we note that it is still possible to compute net power flows such as (52) by considering the limiting value of the net power flow as $\beta \to 1$, which is well-defined because the singularities in $p^E_{x,y}$ and $p^W_{x,y+1}$ for $\beta = 1$ exactly cancel.

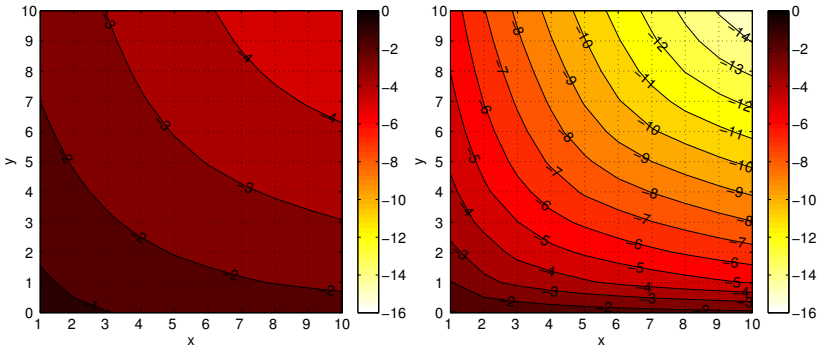

(a) $\beta = 0.9$ (b) $\beta = 0.4$

Figure 14: Contour plots of $\log_{10} W^E_{x,y}$ (defined in (53)) for two values of β. Here the street width $w = 1$.

7. A network of 3D corridors

The model proposed in §3-6 can also be used to describe the propagation of sound from a point source in a network of 3D corridors. We first illustrate this in the case of a single corridor. With lengths nondimensionalised by the width of the corridor, we denote the height of the corridor by h and assume a point source at $(0, y_0, z_0)$ with $0 < y_0 < 1$ and $0 < z_0 < h$. To deal with the wall and floor/ceiling reflections we introduce a doubly-infinite array of image sources at the points $(0, y_n, z_m)$, $n, m \in \mathbf{Z}$, where y_n are defined as in (10) and

$$z_m = \begin{cases} hm + z_0, & m \text{ even}, \\ hm + (h - z_0), & m \text{ odd}. \end{cases} \tag{70}$$

Assume that the floor and ceiling are perfectly reflecting, and that the contributions from the image sources can be summed incoherently. Then, for each $n \in \mathbb{Z}$, the total contribution from the image sources $(0, y_n, z_m)$, $m \in \mathbb{Z}$, to the power flow across the corridor cross-section at distance x from the source is equal to the power flow from the source across the strip $\{x\} \times (0, 1) \times (-\infty, \infty)$. This, in turn, is proportional to the Θ_n, the angular width of the ray tube from the nth image source in the corresponding 2D problem, as defined in §3.

By generalising this argument, one can reduce the calculation of a power flow across a corridor cross-section in a network of 3D corridors to the calculation of a power flow in a corresponding network of 2D streets. Propagation in corridors has been studied previously in [15], via a modal decomposition approach. However, in [15] only the case of a single junction between corridors with perfectly-reflecting walls was considered. A detailed comparison of [15] and the present work can be found in [10, §3.6.5]. We simply note here that explicit evaluation of our integral approximation (27) in the case $\alpha = 0$ gives

$$P^E \sim \frac{1}{2\pi} \left(2 \arctan \frac{1}{w} - w \log \left(1 + \left(\frac{1}{w} \right)^2 \right) \right), \quad l \to \infty, \ \ w = O(1), \tag{71}$$

which agrees exactly with the formula obtained in [15, §II]. Our model therefore generalises the results of [15] to incorporate the effect of multiple junctions and wall absorption.

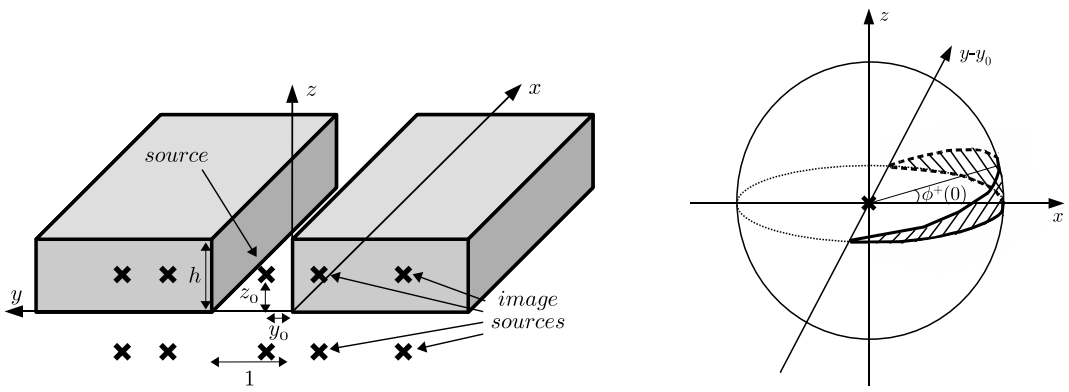

(a) Problem geometry and image source configuration (b) Projection onto the unit sphere

Figure 15: A single street in 3D

8. A 3D urban environment

We now discuss the generalisation of the results of the preceding sections to 3D urban environments. The main ways in which the 3D problem differs from the 2D case are the higher rate of geometrical spreading, the presence of a ground reflection, and the fact that energy emitted from the source can escape to the atmosphere.

8.1. Ray approximation in a single street

As a simple model of a single street in 3D, we consider an infinitely-long channel running parallel to the x-axis, as illustrated in Figure 15(a). After nondimensionalising lengths by the street width, the street is bounded by buildings $(-\infty,\infty)\times(-\infty,0)\times(0,h)$ and $(-\infty,\infty)\times(1,\infty)\times(0,h)$, where $h>0$ is the (nondimensional) building height, assumed constant along the length of the street, and a rigid ground $(-\infty,\infty)\times(0,1)\times\{0\}$. We assume that a point source is located within the street at $(0,y_0,z_0)$, where $0<y_0<1$ and $0<z_0<h$.

As in the 2D case, we simplify the analysis by neglecting the effects of diffraction, and consider the contribution of the multiply-reflected field alone. This can be computed by the introduction of image sources at the points $(0,y_n,\pm z_0)$, $n\in\mathbb{Z}$, with y_n defined as in (10) (see Figure 15(a)). We note that although a ray can undergo an arbitrarily large number of reflections in the walls of the street, no ray undergoes more than one ground reflection. The field is then approximated by

$$\phi\sim-\frac{1}{4\pi}\sum_{z\in\mathbf{Z}}\frac{\mathrm{e}^{ikr_n^-}}{r_n^-}+\frac{\mathrm{e}^{ikr_n^+}}{r_n^+}, \tag{72}$$

where $r_n^\pm=\sqrt{x^2+(y-y_n)^2+(z\pm z_0)^2}$. For simplicity we consider only the case where the source is close enough to the ground to ensure that the interference between each image source and its corresponding ground-reflected image source in (72) is entirely constructive (the general case would require a more careful treatment of the ground reflection, and will not be considered here). Each pair of image sources at $(0,y_n,\pm z_0)$ can then be replaced by a single image source at $(0,y_n,0)$ of

double the amplitude (four times the power output), so that

$$\phi \sim -\frac{1}{2\pi} \sum_{z \in \mathbf{Z}} \frac{\mathrm{e}^{ikr_n}}{r_n}, \tag{73}$$

where $r_n = \sqrt{x^2 + (y - y_n)^2 + z^2}$. It is shown in [10, §3.9.1] that for (73) to hold it is sufficient to assume that $x \gg 1/k$ (so we are not too close to the source) and that $z_0 \ll x/(kh)$.

8.2. The acoustic power flow in a single street

As in the 2D case, we assume that the intensity contributions from the infinitely many image sources in (73) can be summed incoherently, with the effect of interference being neglected. The power flow P across the street cross-section $\{x\} \times (0, 1) \times (0, h)$, as a fraction of the total free space power output of the source, is then

$$P = \frac{1}{\pi} \sum_n (1 - \alpha)^{|n|} \tilde{\Omega}_n, \tag{74}$$

where α is the absorption coefficient of the walls and $\tilde{\Omega}_n$ is the solid angle subtended at the source by the ray tube incident on the nth image street cross-section. In terms of the spherical coordinates

$$x = \cos\phi \cos\theta, \qquad y - y_0 = \cos\phi \sin\theta, \qquad z = \sin\phi,$$

where the angle ϕ represents 'latitude' on the unit sphere (so that ϕ equals $\pi/2$ minus the usual spherical polar angle), we have

$$\tilde{\Omega}_n = \int_{\tilde{\theta}_n^-}^{\tilde{\theta}_n^+} \int_0^{\phi^+(\theta)} \cos\phi \, d\phi d\theta, \tag{75}$$

where $\tilde{\theta}_n^{\pm}$ are defined as in (15) and $\phi^+(\theta) = \arctan\left((h\cos\theta)/x\right)$. The ϕ-integration in (75) is trivial, and

$$\tilde{\Omega}_n = \int_{\tilde{\theta}_n^-}^{\tilde{\theta}_n^+} \sin\left(\phi^+(\theta)\right) d\theta = \int_{\tilde{\theta}_n^-}^{\tilde{\theta}_n^+} \frac{1}{\sqrt{1 + \left(\frac{x}{h\cos\theta}\right)^2}} \, d\theta.$$

In the special case $\alpha = 0$ the sum (74) is telescoping, and

$$P = \frac{2}{\pi} \int_0^{\pi/2} \frac{1}{\sqrt{1 + \left(\frac{x}{h\cos\theta}\right)^2}} \, d\theta = \frac{2}{\pi} \arctan\frac{h}{x}.$$

In this case P is proportional to the power flow due to a single source at $(0, y_0, 0)$ across the infinite strip $C = \{x\} \times (-\infty, \infty) \times (0, h)$, which, in turn, is proportional to the area of the segment formed by the projection of C onto the unit sphere centred at $(0, y_0, 0)$ - see Figure 15(b). There is a bias towards rays with small θ, since these rays gain less height with every unit travelled in the x-direction than those with larger θ. Note that when $x \gg h$ we have

$$P \sim \frac{2h}{x\pi}, \tag{76}$$

and the decay in power due to losses to the atmosphere is found to be *algebraic* in the distance down the street.

More generally, when $x \gg 1$ and $\alpha \ll 1$ we may, as in the 2D case, approximate the sum (74) by an integral:

$$P \sim \frac{2}{\pi} \int_0^{\pi/2} \frac{(1-\alpha)^{x \tan\theta}}{\sqrt{1 + \left(\frac{x}{h \cos\theta}\right)^2}} \, d\theta. \tag{77}$$

When also $x \gg h$, (77) can be further approximated to give

$$P \sim \frac{2h}{x\pi} \int_0^{\pi/2} (1-\alpha)^{x \tan\theta} \cos\theta \, d\theta. \tag{78}$$

8.3. Acoustic power flows in a network of streets

In this section we propose a method for estimating acoustic power flows across street cross-sections in a network of streets in 3D, which generalises that developed in §3-6 for the 2D problem. We first introduce the method in general terms, then illustrate it in a number of examples, comparing the results to those for the corresponding 2D problems. We assume for simplicity that the buildings all have equal height h.

Suppose that, as a fraction of the total free space power output of the source, the power flow P across a particular street cross-section is given by a ray tube sum of the form

$$P = \frac{1}{\pi} \sum_n B_n \tilde{\Omega}_n. \tag{79}$$

Here B_n represents the effect of wall absorption, and will be the same as in the analogous 2D problem. $\tilde{\Omega}_n$ is the solid angle subtended by the nth ray tube at the source location,

$$\tilde{\Omega}_n = \int_{\tilde{\theta}_n^-}^{\tilde{\theta}_n^+} \int_0^{\phi^+(\theta)} \cos\phi \, d\phi d\theta, \tag{80}$$

where $\tilde{\theta}_n^{\pm}$ are the launch angles of the rays bounding the corresponding ray tube in the analogous 2D problem, and $\phi^+(\theta) = \arctan\left(h/L(\theta)\right)$, where $L(\theta)$ is the length of a ray of launch angle θ reaching the street cross-section in the analogous 2D problem. The ϕ-integration in (80) is trivial, so that

$$\tilde{\Omega}_n = \int_{\tilde{\theta}_n^-}^{\tilde{\theta}_n^+} G(\theta) \, d\theta,$$

where

$$G(\theta) = \sin\phi^+(\theta) = \left(1 + \left(L(\theta)/h\right)^2\right)^{-1/2}. \tag{81}$$

We then propose to approximate (79) by the integral

$$P_{\text{app}} := \frac{2}{\pi} \int_0^{\pi/2} A(\theta) F(\theta) G(\theta) \, d\theta, \tag{82}$$

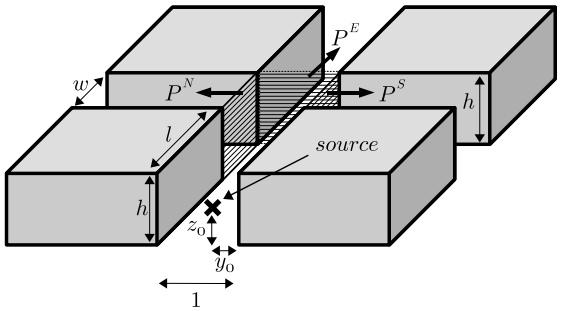

(a) Problem geometry

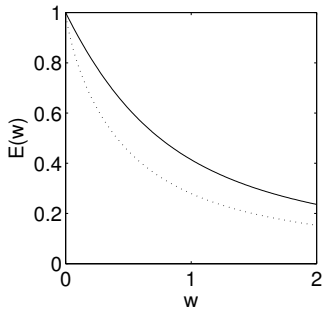

(b) the functions E_{3D} (solid) and E_{2D} (dotted)

Figure 16: A crossroads in 3D.

where the absorption factor $A(\theta)$ and the energy redistribution factor $F(\theta)$ are exactly as in the analogous 2D problem. We expect (82) to provide a good approximation to (79) only when the streets in the network are long and the typical absorption coefficient is small. Furthermore, when multiple junctions are involved, we conjecture, as in the 2D case, that the approximations represent *expected* power flows after averaging over a suitable range of street lengths. Note that when also $L(\theta) \gg h$ we can further approximate $G(\theta) \sim h/L(\theta)$ to give

$$P_{\text{app}} \sim \frac{2h}{\pi} \int_0^{\pi/2} \frac{A(\theta)F(\theta)}{L(\theta)}\, d\theta. \tag{83}$$

One example, the power flow in a single street, has already been considered in §8.2. In this case,

$$B_n = (1-\alpha)^{|n|}, \qquad A(\theta) = (1-\alpha)^{x\tan\theta}, \qquad F(\theta) = 1, \qquad L(\theta) = \frac{x}{\cos\theta}.$$

We now consider a number of other examples.

8.4. Energy redistribution at a crossroads

Consider the case of a right-angled crossroads, where a street of width w intersects a main street at a distance l from the source (see Figure 16(a)). In the ray tube sum (79) for the power flow P^E out of the East exit we have $B_n = (1-\alpha)^{|n|}$, and $\tilde{\theta}_n^{\pm}$ are now defined as in (25). Accordingly, in the integral approximations (82) and (83) we have

$$A(\theta) = (1-\alpha)^{l\tan\theta}, \qquad F(\theta) = F_C(\theta; w), \qquad L(\theta) = \frac{l}{\cos\theta}.$$

When $l \gg h$, (83) then gives

$$P^E_{\text{app}} \sim \frac{2h}{\pi l} \int_0^{\pi/2} (1-\alpha)^{l\tan\theta} F_C(\theta; w)\cos\theta\, d\theta. \tag{84}$$

It is interesting to compare (84) with the corresponding 2D result (29). For simplicity we assume that $\alpha = 0$; in this special case the integral in (84) can be evaluated explicitly to give

$$P^E_{\text{app}} = \frac{2h}{\pi l}\left(\sqrt{1+\left(\frac{w}{2}\right)^2} - \frac{w}{2}\right).$$

By comparison with (76), we see that the prefactor $2h/(\pi l)$ in (84) represents the power incident on the junction. Thus the fraction E_{3D} of energy incident on the junction that carries on down the main street is given as a function of w by

$$E_{3D}(w) = \int_0^{\pi/2} F_C(\theta; w) \cos\theta \, d\theta.$$

The corresponding expression in 2D is

$$E_{2D}(w) = \frac{2}{\pi} \int_0^{\pi/2} F_C(\theta; w) \, d\theta.$$

A plot of the functions E_{2D} and E_{3D} is presented in Figure 16(b). Note that in 3D a greater proportion of the incident energy passes the junction than in 2D. This is because in 3D the energy incident on the junction is not distributed uniformly over all $\theta \in (0, \pi/2)$, as it is in the two dimensional case; rather there is a bias towards rays with small θ, as remarked at the end of §8.2 (and see Figure 15(b)). Such rays contribute more to the power flow than those with larger θ because $F_C(\theta, w)$ is a decreasing function of θ.

8.5. A two-junction environment

As a further example, we consider the 3D analogue of the 2D two-junction environment illustrated in Figure 12(a), for which the approximations (39) and (40) were obtained. In the 3D case the integral approximation (82) of the power flows $P^E(2)$ and $P^W(2)$ would have

$$A(\theta) = (1-\alpha_0)^{l_0 \tan\theta} (1-\alpha_1)^{\frac{l_1}{w_1} \tan(\pi/2-\theta)}, \tag{85}$$

$$F(\theta) = F_T(\theta; w_1) F_T\left(\pi/2 - \theta; \frac{w_2}{w_1}\right), \tag{86}$$

$$L(\theta) = \frac{l_0}{\cos\theta} + \frac{l_1}{\cos(\pi/2-\theta)}, \tag{87}$$

and to obtain the integral approximation of $P^N(2)$ we would replace (86) by

$$F(\theta) = F_T(\theta; w_1) F_C\left(\pi/2 - \theta; \frac{w_2}{w_1}\right).$$

8.6. A network of streets

The integral approximation method can be used to estimate the power flows in a network of streets in 3D. For simplicity we consider the case of a regular network in which the street length l, width w, and height h are constant across the network, and there is no wall absorption. We also assume that $l \gg h$ so that the simplified form (83) applies, although we expect similar results in the more general case.

As in the 2D case, estimates of net power flows can be obtained by considering only those paths which have minimal length. Defining $P^E_\lambda(N)$ as in (42), we may investigate the behaviour of $P^E_\lambda(N)$ for large N. For simplicity we consider only the cases $\lambda = 0, 1/2$; in both cases there is only one path of minimal length.

- When $\lambda = 0$ we have

$$F(\theta) = F_C(\theta; 1)^N, \qquad L(\theta) = \frac{Nl}{\cos\theta},$$

and our estimate for $P_0^E(N)$ is

$$P_0^E(N) = \frac{2h}{\pi N l} \int_0^{\pi/4} \exp\left[N \log\left(1 - \tan\theta\right)\right] \cos\theta \, d\theta.$$

We find that

$$P_0^E(N) \sim \frac{2h}{\pi N^2 l}, \quad N \to \infty,$$

so that the decay is *algebraic* in the number of junctions encountered.

- Along the diagonal $\lambda = 1/2$ (with N even) we have

$$F(\theta) = F_C(\theta; 1)^{N/2} F_T\left(\pi/2 - \theta; 1\right)^{N/2}, \qquad L(\theta) = \frac{Nl}{2}\left(\frac{1}{\cos\theta} + \frac{1}{\sin\theta}\right),$$

and our estimate for $P_{1/2}^E(N)$ is

$$P_{1/2}^E(N) = \frac{8h}{\pi N l} \int_0^{\pi/4} \exp\left[N\left(\frac{1}{2}\log\left(\frac{\tan\theta}{4}\right)\right)\right] \frac{1}{\left(\frac{1}{\cos\theta} + \frac{1}{\sin\theta}\right)} \, d\theta.$$

We find that

$$P_{1/2}^E(N) \sim \frac{2\sqrt{2}h}{\pi N^2 l}\left(\frac{1}{2}\right)^N, \quad N \to \infty, \ (N \text{ even}),$$

so that the decay is *exponential* in the number of junctions encountered.

It is not clear whether the integral approximations derived here can be used to formulate a partial difference equation model analogous to that proposed for the 2D case in §6.2. There we were able to relate the θ-resolved power flows into one junction to the θ-resolved power flows out of the neighbouring junctions. This formulation relies crucially on the fact that the absorption and energy redistribution factors $A(\theta)$ and $F(\theta)$ in our integral approximations are 'multiplicative', in the sense that $A(\theta)$ and $F(\theta)$ are multiplied by a factor at each additional street/junction encountered. In the 3D case, however, the factor $G(\theta)$ in the integrand in (82) does not follow the same rule. Indeed, the length $L(\theta)$ appearing in (81) is 'additive', in the sense that with each additional street/junction encountered, we must add a term to $L(\theta)$, rather than multiply it by a factor. Whether these difficulties can be resolved is still an open question, and we leave any further discussion of these issues for future work.

9. Conclusions

We have derived a model for the propagation of acoustic energy from a time-harmonic point source through a network of interconnecting streets. Our model represents the power flow along any

pathway through the network as the integral of a power density over the launch angle of a ray emanating from the source. The dependence of the power density on the launch angle takes into account the key phenomena involved in the propagation, namely energy loss by wall absorption, energy redistribution at junctions, and, in 3D, energy loss to the atmosphere. We have shown, by means of a number of examples, how the power density for a given propagation pathway may be explicitly computed.

Computing the total net power flow across a street cross-section requires the summation of the power flows along each of propagation pathways from the source. An estimate can be obtained by considering only paths of minimal length. In 2D the full summation can be computed implicitly, by formulating a system of partial difference equations for the power densities flowing out of the exits of each junction in the network. In a special case we were able to obtain an exact solution to this system. However, the generalisation of this formulation to the 3D case remains an area for future research.

In summary, our model predicts strongly anisotropic decay away from the source, with the power flow decaying exponentially in the number of junctions from the source, except along the axial directions of the network, where the decay is algebraic. The model is not only concerned with the calculation of acoustic power flows - once the power density has been determined, an elementary modification of the integral allows us to compute the acoustic energy density and the mean-square pressure, averaged over the street cross-section.

10. Acknowledgements

The author would like to thank Prof. J. R. Ockendon, Dr D. J. Allwright and Prof. C. J. Chapman for their helpful comments, and gratefully acknowledges the support of the EPSRC and Dstl (MOD research programme, contract RD023-2985).

References

[1] F. M. Wiener, C. I. Malme, C. M. Gogos, Sound propagation in urban areas, J. Acoust. Soc. Am. 37 (4) (1965) 638–747.

[2] R. H. Lyon, Role of multiple reflections and reverberation in urban noise propagation, J. Acoust. Soc. Am. 55 (3) (1974) 493–503.

[3] H. G. Davies, Multiple-reflection diffuse-scattering model for noise propagation in streets, J. Acoust. Soc. Am. 64 (2) (1978) 517–521.

[4] K. K. Iu, K. M. Li, The propagation of sound in narrow street canyons, J. Acoust. Soc. Am. 112 (2) (2002) 537–550.

[5] J. Kang, Sound propagation in street canyons: comparison between diffusely and geometrically reflecting boundaries, J. Acoust. Soc. Am. 107 (2000) 1394–1404.

[6] R. Bullen, F. Fricke, Sound propagation in a street, J. Sound Vib. 46 (1) (1976) 33–42.

[7] A. Pelat, S. Félix, V. Pagneux, On the use of leaky modes in open waveguides for the sound propagation modeling in street canyons, J. Acoust. Soc. Am. 126 (2009) 2864–2872.

[8] J. Picaut, L. Simon, J. Hardy, Sound field modelling in streets with a diffusion equation, J. Acoust. Soc. Am. 106 (5) (1999) 2638–2645.

[9] T. Le Pollès, J. Picaut, M. Bérengier, C. Bardos, Sound field modeling in a street canyon with partially diffusely reflecting boundaries by the transport theory, J. Acoust. Soc. Am. 116 (5) (2004) 2969–2983.

[10] D. P. Hewett, Sound propagation in an urban environment, DPhil thesis, University of Oxford, 2010.

[11] J. Kang, Urban Sound Environment, Taylor and Francis, 2006.

[12] R. H. Lyon, Propagation of environmental noise, Science 179 (1973) 1083–1090.

[13] K. Attenborough, K. M. Li, K. Horoshenkov, Predicting Outdoor Sound, Taylor and Francis, 2006.

[14] R. Bullen, F. Fricke, Sound propagation at a street intersection in an urban environment, J. Sound Vib. 54 (1) (1977) 123–129.

[15] H. G. Davies, Noise propagation in corridors, J. Acoust. Soc. Am. 53 (5) (1973) 1253–1262.

[16] M. Crocker, Handbook of Noise and Vibration Control, John Wiley and Sons, 2007.

[17] J. B. Keller, Geometrical theory of diffraction, J. Opt. Soc. Am. 52 (2) (1962) 116–130.

[18] V. A. Borovikov, B. Y. Kinber, Geometrical Theory of Diffraction, The Institution of Electrical Engineers, 1994.

[19] F. Fahy, Sound Intensity, Taylor and Francis, 1995.

[20] C. H. Hodges, J. Woodhouse, Theories of noise and vibration transmission in complex structures, Rep. Prog. Phys. 49 (1986) 107–170.

[21] M. J. Lighthill, Waves in Fluids, Cambridge University Press, 2003.

[22] A. G. Galitsis, W. N. Patterson, Prediction of noise distribution in various enclosures from free-field measurements, J. Acoust. Soc. Am. 60 (4) (1976) 848–856.

[23] W. A. Kinney, A. D. Pierce, R. E. J., Helicopter noise experiments in an urban environment, J. Acoust. Soc. Am. 56 (2) (1974) 332–337.

[24] R. H. Lyon, R. G. DeJong, Theory and Application of Statistical Energy Analysis, Butterworth-Heinemann, 1995.

[25] M. E. Delany, E. N. Bazley, Monopole radiation in the presence of an absorbing plane, J. Sound Vib. 13 (3) (1970) 269–279.

[26] M. Gensane, F. Santon, Prediction of sound fields in rooms of arbitrary shape: validity of the image sources method, J. Sound Vib. 63 (1) (1979) 97–108.

[27] U. Ingard, On the reflection of a spherical sound wave from an infinite plane, J. Acoust. Soc. Am. 23 (3) (1951) 329–335.

[28] M. A. Nobile, S. I. Hayek, Acoustic propagation over an impedance plane, J. Acoust. Soc. Am. 78 (4) (1985) 1325–1336.

[29] H. Shirai, L. B. Felsen, Rays, modes and beams for plane wave coupling into a wide open-ended parallel-plane waveguide, Wave Motion 9 (2) (1987) 301–317.

[30] H. Y. Yee, L. B. Felsen, J. B. Keller, Ray theory of reflection from the open end of a waveguide, SIAM J. App. Math. 16 (2) (1968) 268–300.

[31] B. van der Pol, H. Bremmer, Operational Calculus based on the two-sided Laplace Integral, Cambridge University Press, 1950.

[32] E. J. Watson, Infinite regular electrical networks, Eur. J. Appl. Math. 16 (5) (2005) 555–567.